J. Micropalaeontology, 43, 165–186, 2024
https://doi.org/10.5194/jm-43-165-2024

Journal of Micropalaeontology
Open Access

South Georgia marine productivity over the past 15 ka and implications for glacial evolution

Jack T. R. Wilkin[1,2], Sev Kender[1,3], Rowan Dejardin[4], Claire S. Allen[2], Victoria L. Peck[2], George E. A. Swann[5], Erin L. McClymont[6], James D. Scourse[1], Kate Littler[1,7], and Melanie J. Leng[3,8]

[1]Department of Earth and Environmental Sciences, University of Exeter, Penryn, TR10 9EZ, UK
[2]British Antarctic Survey, Cambridge, CB3 0ET, UK
[3]British Geological Survey, Nottingham, NG12 5GG, UK
[4]School of Geographical Sciences, University of Bristol, Bristol, BS8 1SS, UK
[5]School of Geography, University of Nottingham, University Park, Nottingham, NG7 2RD, UK
[6]Department of Geography, Durham University, Durham, DH1 3LE, UK
[7]Environment and Sustainability Institute, University of Exeter, Penryn, TR10 9EZ, UK
[8]School of Biosciences, University of Nottingham, Loughborough, NE12 5RD, UK

Correspondence: Jack T. R. Wilkin (jack.wilkin@btinternet.com, jw923@exeter.ac.uk)

Received: 21 December 2023 – Revised: 30 April 2024 – Accepted: 2 May 2024 – Published: 18 June 2024

Abstract. The subantarctic islands of South Georgia are located in the Southern Ocean, and they may be sensitive to future climate warming. However, due to a lack of well-dated subantarctic palaeoclimate archives, there is still uncertainty about South Georgia's response to past climate change. Here, we reconstruct primary productivity changes and infer Holocene glacial evolution by analysing two marine gravity cores: one near Cumberland Bay on the inner South Georgia shelf (GC673: ca. 9.5 to 0.3 cal. kyr BP) and one offshore of Royal Bay on the mid-shelf (GC666: ca. 15.2 cal. kyr BP to present). We identify three distinct benthic foraminiferal assemblages characterised by the dominance of *Miliammina earlandi, Fursenkoina fusiformis*, and *Cassidulinoides parkerianus* that are considered alongside foraminiferal stable isotopes and the organic carbon and biogenic silica accumulation rates of the host sediment. The *M. earlandi* assemblage is prevalent during intervals of dissolution in GC666 and reduced productivity in GC673. The *F. fusiformis* assemblage coincides with enhanced productivity in both cores. Our multiproxy analysis provides evidence that the latest Pleistocene to earliest Holocene (ca. 15.2 to 10.5 cal. kyr BP) was a period of high productivity associated with increased glacial meltwater discharge. The mid–late Holocene (ca. 8 to 1 cal. kyr BP), coinciding with a fall in sedimentation rates and lower productivity, was likely a period of reduced glacial extent but with several short-lived episodes of increased productivity from minor glacial readvances. The latest Holocene (from ca. 1 cal. kyr BP) saw an increase in productivity and glacial advance associated with cooling temperatures and increased precipitation which may have been influenced by changes in the southwesterly winds over South Georgia. We interpret the elevated relative abundance of *F. fusiformis* as a proxy for increased primary productivity which, at proximal site GC673, was forced by terrestrial runoff associated with the spring–summer melting of glaciers in Cumberland Bay. Our study refines the glacial history of South Georgia and provides a more complete record of mid–late Holocene glacial readvances with robust chronology. Our results suggest that South Georgia glaciers were sensitive to modest climate changes within the Holocene.

Published by Copernicus Publications on behalf of The Micropalaeontological Society.

1 Introduction

South Georgia (∼ 54–55° S, 36–38° W; Fig. 1) lies on the North Scotia Ridge in the eastern Scotia Sea. South Georgia is separated from the deep ocean by 50–150 km of continental shelf typically shallower than 300 m and crossed by submarine troughs (Meredith et al., 2003). South of the polar front, South Georgia is constantly surrounded by polar waters and heavily glaciated, yet sea ice formation is rare (Atkinson et al., 2001; Meredith et al., 2003). The scarcity of landmasses in the subantarctic makes South Georgia and the surrounding shelf (the focus of this study) a prime site to better understand the drivers and impacts of post-deglacial climate change in the subantarctic region (Berg et al., 2019). There are a number of Holocene records documenting South Georgia's past climate from lake and peat cores (Clapperton et al., 1989; van der Putten et al., 2004; Xia et al., 2020; Zwier et al., 2021; van der Bilt et al., 2022) and marine (Graham et al., 2017; Kristan et al., 2022; Lešić et al., 2022) and coastal (Berg et al., 2019) sediment cores. Although marine records provide palaeoceanographic information on the latest Holocene (Kristan et al., 2022), there are so far no continuous early- and mid-Holocene palaeoenvironmental reconstructions from South Georgia shelf records.

Geomorphological evidence indicates that South Georgia was extensively glaciated during the Last Glacial Maximum (LGM; e.g. Clapperton et al., 1989; Bentley et al., 2007; Graham et al., 2008; Hodgson et al., 2014a; Barlow et al., 2016; White et al., 2017). The relatively high diversity of plants during the deglacial implies that some areas of the island remained ice-free during the LGM, with plants surviving in refugia on South Georgia and its adjacent archipelago (Barlow, 1977; van der Putten and Verbruggen, 2005). Exposure dating using ^{10}Be isotopes of glacial erratics suggests that the recession of the LGM ice cap exposed lower elevations around 16 cal. kyr BP (White et al., 2017). Radiocarbon dates from lake sediments from the Tønsberg peninsula (Rosqvist et al., 1999) suggest that the ice retreated from the Cumberland Bay area ca. 15.7 cal. kyr BP (van der Putten and Verbruggen, 2005). This initial ice retreat was interrupted by a major readvance into the outer fjords during the Antarctic Cold Reversal (ACR; 14.7 to 13.0 cal. kyr BP; Pedro et al., 2016; Graham et al., 2017) when South Georgia's temperatures decreased, as evidenced by plant subfossils and palaeoecology (Clapperton et al., 1989; see also Bakke et al., 2021). After the ACR, there is a general trend towards warmer temperatures at the transition between the late Pleistocene and early Holocene.

Since the deglacial, several glacial readvancements have been reported from records restricted to the inner fjords (Clapperton et al., 1989; Rosqvist et al., 1999; Hodgson et al., 2014a, b; Oppedal et al., 2018; Berg et al., 2019; Bakke et al., 2021). The deglaciation of low-altitude sites in the early Holocene is evidenced by the onset of biogenic sedimentation in lakes and peat bog sediment cores (van der Putten and Verbruggen, 2005; Hodgson et al., 2014a). Peat bog deposition around Cumberland Bay commenced around 11.6 to 10.5 cal. kyr BP (van der Putten and Verbruggen, 2005), with evidence that possible glacial readvances occurred during this period (Clapperton et al., 1989). The mid-Holocene (7.5 to 2.9 cal. kyr BP), often interpreted as a "climatic optimum", with higher temperatures followed by cooling and glacial readvancement ca. 5.0 to 0.3 cal. kyr BP is sometimes referred to as the "Neoglacial" (Clapperton et al., 1989).

During the Neoglacial (3 to 2 kyr BP; Clapperton et al., 1989), evidence for widespread growth of glaciers on South Georgia has been reported (e.g. Clapperton et al., 1989; Bentley et al., 2007; Roberts et al., 2010; van der Bilt et al., 2017; White et al., 2017; Oppedal et al., 2018; Berg et al., 2019). Late Holocene glacial readvances (ca. 2.9 cal. kyr BP onwards) appear to have been less extensive than those from the mid-Holocene (7.5 to 2.9 cal. kyr BP) and may have exhibited variability on centennial timescales (van der Bilt et al., 2017; Berg et al., 2019). Covariance of Patagonian and South Georgian glacier fluctuations may indicate a shared regional climate forcing (Strelin et al., 2014). One such forcing is changes in the southern westerly winds (SWWs), which have a major impact on precipitation rates and temperature (Mayr et al., 2007; Lamy et al., 2010; Perren et al., 2020; Fletcher et al., 2021; Zwier et al., 2021; Spoth et al., 2023). However, there is significant uncertainty about the precise timing of South Georgia Holocene glacial readvances, making it difficult to test this common forcing idea or assess the impact South Georgia's glacial history had on the marine realm.

Here, we present two continuous multiproxy records from two sediment cores from the South Georgia's continental shelf, chronologically constrained with radiocarbon dating. The principal goal of this paper is to reconstruct the palaeoenvironment of South Georgia and to assess changes to marine productivity and sediment delivery to the inner (CG673) to mid-shelf (GC666). Seasonal glacial melt and the resultant high delivery of nutrient-rich glacial outwash is thought to be a dominant source of iron delivery around South Georgia (Hodgson et al., 2017; Schlosser et al., 2018). Proxy records for past productivity can therefore be used to infer seasonal meltwater flux, and in turn glacial extent, in South Georgia bays. By analysing benthic foraminiferal assemblages, organic carbon, and biogenic silica accumulation rates (C_{org} AR and BSi AR respectively), we are able to reconstruct relative changes in the latest Pleistocene and Holocene primary productivity. We propose that episodes of enhanced productivity in the middle–late Holocene at nearshore GC673 occurred during glacial advances.

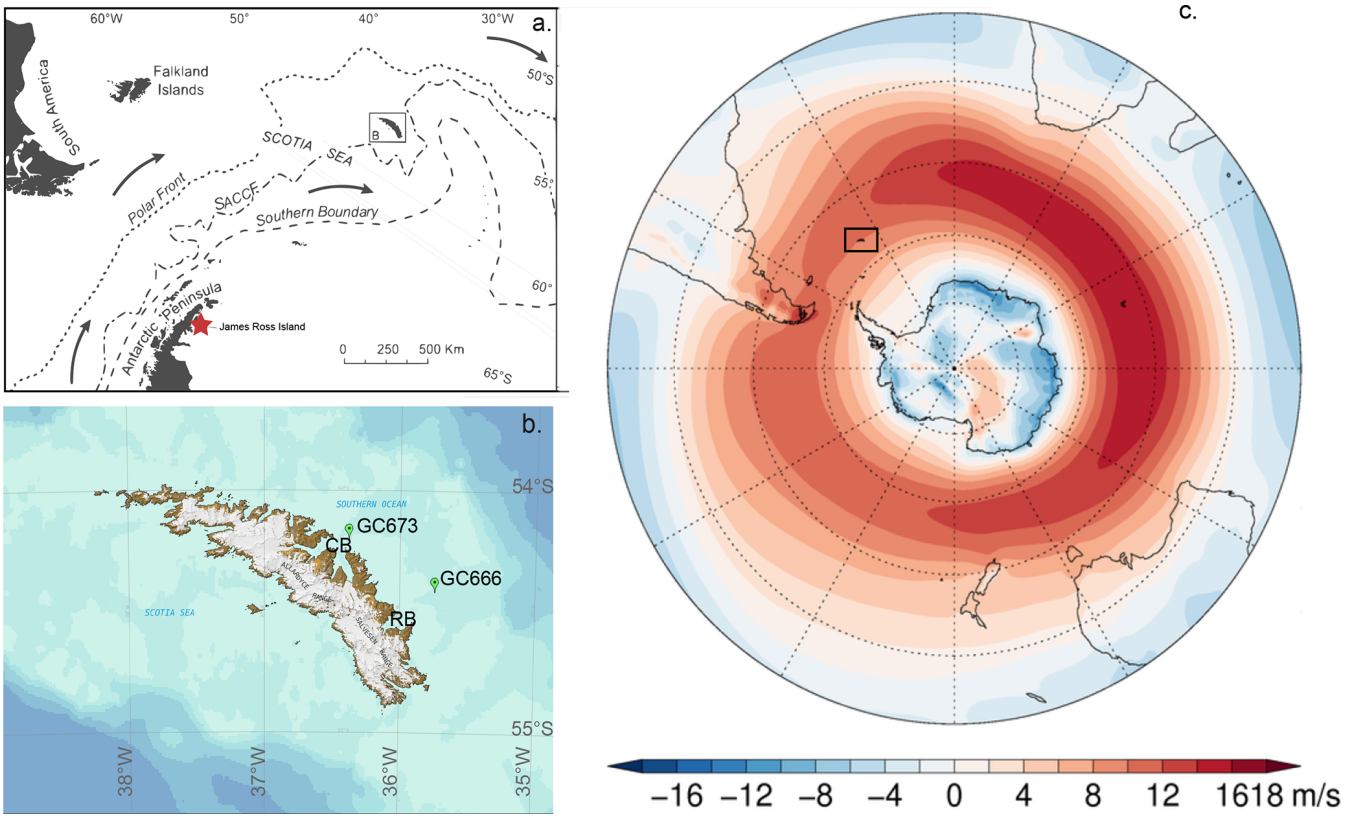

Figure 1. Sample location map. **(a)** The South Atlantic sector of the Southern Ocean, showing the position of South Georgia (boxed), the location of the ice core from James Ross island (red star), and the positions of the main frontal systems which influence South Georgia's climate. SACCF is the Southern Antarctic Circumpolar Current Front. **(b)** Topographic map of South Georgia showing the surrounding bathymetry with locations of the two studied cores created using the South Georgia Geographic Information System (https://sggis.gov.gs/, last access: 6 April 2023). GC673 is located offshore of Cumberland Bay and GC666 offshore of Royal Bay. **(c)** Southern Hemisphere tropospheric westerly jet from 1979–2018 (Bracegirdle, 2018). CB is for Cumberland Bay; RB is for Royal Bay. Publisher's remark: please note that the above figure contains disputed territories.

2 Methods and materials

2.1 Material

Two marine sediment gravity cores (GCs), were collected during the British Antarctic Survey scientific cruise JR-257 in April 2012, on Royal Research Ship (RRS) *James Clark Ross* (Allen et al., 2012). They are part of a transect of marine sediment cores spanning the South Georgia continental shelf selected to reconstruct the local glaciological history, including the former grounded ice cap extent. The study cores come from the northern ends of cross-shelf troughs that propagate from Royal Bay (GC666) and Cumberland Bay (GC673) on the northern part of the South Georgia shelf (Table 1 and Fig. 1).

The cores were collected using a gravity corer made up of a combination of 3 and 6 m long steel barrels with a bomb weight at the top end, allowing barrel configurations with a range of lengths to be deployed. GC666 was recovered from a 12 m deployment, and GC673 was recovered from a 15 m deployment. Pre-labelled core liners were inserted into the barrels, followed by a polyethylene-bag-lined core catcher. The complete corer assembly was deployed to the seafloor by the midship winch. After recovery, the core was cut into approximately 1 m sections; each section was capped at both ends, cleaned, and then transferred to a cool store.

The core sections were then split at the Alfred Wegener Institute in Bremerhaven, Germany (GC666), and the British Antarctic Survey in Cambridge, UK (GC673). Both GC666 and GC673 were sampled at 1 cm resolution, with samples bagged, labelled, and freeze-dried with Thermo ModuloyD freeze dryers at the University of Nottingham.

At the site of GC666, a distinct facies change can be seen in acoustic profiles (Graham et al., 2017) which corresponds to changes in sediment types (originally described by Graham et al., 2017). Five radiocarbon dates from GC666 had previously been published by Graham et al. (2017), which we have added to nine new dates to create our new age model. Unit 1 forms the basal section of the core from 816 to 500 cm core depth (cmcd) and is a biologically productive glacially

Table 1. Cores analysed in this study. m b.s.l.is for metres below sea level.

Core	Latitude (° S)	Longitude (° E)	Depth (m b.s.l.)	Cruise	Length of core (m)
GC666	54.4206	−35.74148	253	JR-257	8.15
GC673	54.20237	−36.37451	238	JR-257	8.84

influenced marine environment comprised of laminated diatomaceous mud with a high sedimentation rate which we calculated to have been ca. 500 cm kyr^{-1} (Fig. 2). The laminated sediments consist of diatomaceous oozes alternating with fine-grained, more terrigenous diatom-rich muds interpreted to record inter-annual or perhaps even seasonal deposition in an open-marine setting (Graham et al., 2017). Units 1 and 2 are separated by a ca. 5 cm thick carbonate cemented mud. Unit 2 (500 to 0 cmcd) is a less productive hemipelagic shelf environment comprised of grey/olive green homogeneous sandy diatomaceous mud throughout with dark mottles and intermittent dropstones. The higher terrestrial sediment content in Unit 2 may be due to a dilution effect rather than an indicator of supply (Graham et al., 2017). The sedimentation rate for Unit 2 ranges from 4 to 125 cm kyr^{-1} based on our new age model (Fig. 2).

GC673 has a higher percentage of terrigenous sediments, comprised a single unit of grey/olive green sandy bioturbated diatomaceous mud with no notable sedimentological changes (Fig. 2). Occasional thin dark green or orange laminae, interpreted as diatomaceous ooze, are recorded throughout the core, in particular between 883–620 cmcd and 210–0 cmcd. Dropstones are also intermittently present, and there is an increase in sand at ca. 350 cmcd. Inclusions of carbonate cemented mud several centimetres in diameter were recorded at 672 and 760 cmcd.

2.2 Dating

Age–depth models for the cores were generated using a total of 18 radiocarbon dates (Fig. 1). The source of the carbonate used was non-agglutinated foraminifera and bivalve shell fragments. For the horizons analysed as part of this study, samples (4–12 µg) of mixed assemblage benthic foraminifera were picked from the > 125 µm sediment fraction. Five radiocarbon dates from GC666 had previously been published by Graham et al. (2017). We collected an additional nine samples for radiocarbon dating from GC666 which were graphitised and analysed at the Poznan Radiocarbon Laboratory, Adam Mickiewicz University, Poland, using a 1.5 SDH Pelletron model "compact carbon AMS" system with an MC-SNICS ion source. Four radiocarbon samples from GC673 were graphitised and analysed at the Natural Environment Research Council (NERC) Radiocarbon Facility, East Kilbride, UK, using an NEC accelerator mass spectrometer (AMS). For some samples, combining benthic foraminifera from two to four adjacent samples was necessary to have enough material to generate accurate dates.

The ^{14}C ages were calibrated to BP (Before Present – 1950) using BChron, a Bayesian chronology model implemented in R (Haslett and Parnell, 2008) with the Marine20 calibration curve applied (Heaton et al., 2020). A local reservoir correction (δR) of 433 ± 41 years was used, based on the age of surface sediments from a box core (BC671) reported by Dejardin (2017), in preference to the δR of 708 ± 61 years applied by Graham et al. (2017). Age–depth modelling as per the algorithm of Haslett and Parnell (2008) for both cores was generated using BChron with interpolated BP dates generated at 1 cm resolution and sediment accumulation rates calculated.

It is important to always consider the associated uncertainties when applying the ages generated by these modelling techniques, especially when discussing the relationship between changes in the proxy records developed here and climate events with well-established dates. Although there is a large uncertainty associated with the modelled ages through this period, the 2σ uncertainty in the modelled ages generated for GC666 ranges from ± 165 years to ± 442 years (mean $= \pm 331$ years), and the 2σ is much higher outside of the four dated horizons. The 2σ uncertainty in the modelled ages generated for GC673 ranges from ± 188 years to ± 2513 years (mean $= \pm 874$ years), and the 2σ is much higher outside of the four dated horizons. There is also some uncertainty regarding the accuracy of the local reservoir correction which has been based on a single modern sample. Furthermore, it is not possible to quantify how this reservoir effect may have varied through time, a factor that may not be important in the Holocene but can be considerable over the transitions between glacial and interglacial (Skinner et al., 2019; Heaton et al., 2020). The diagenetic alteration of foraminifera in the lower part of both cores, potentially due to methane activity (see Sect. 4), also has the potential to impact radiocarbon dates. Specimens with suspected authigenic carbon precipitation were therefore not selected for radiocarbon analysis. Although dated foraminifera were selected from specimens with no visual signs of alteration, ages reported for samples where diagenetic alteration has been identified may be older than their true ages (e.g. Pohlman et al., 2013; Wycech et al., 2016).

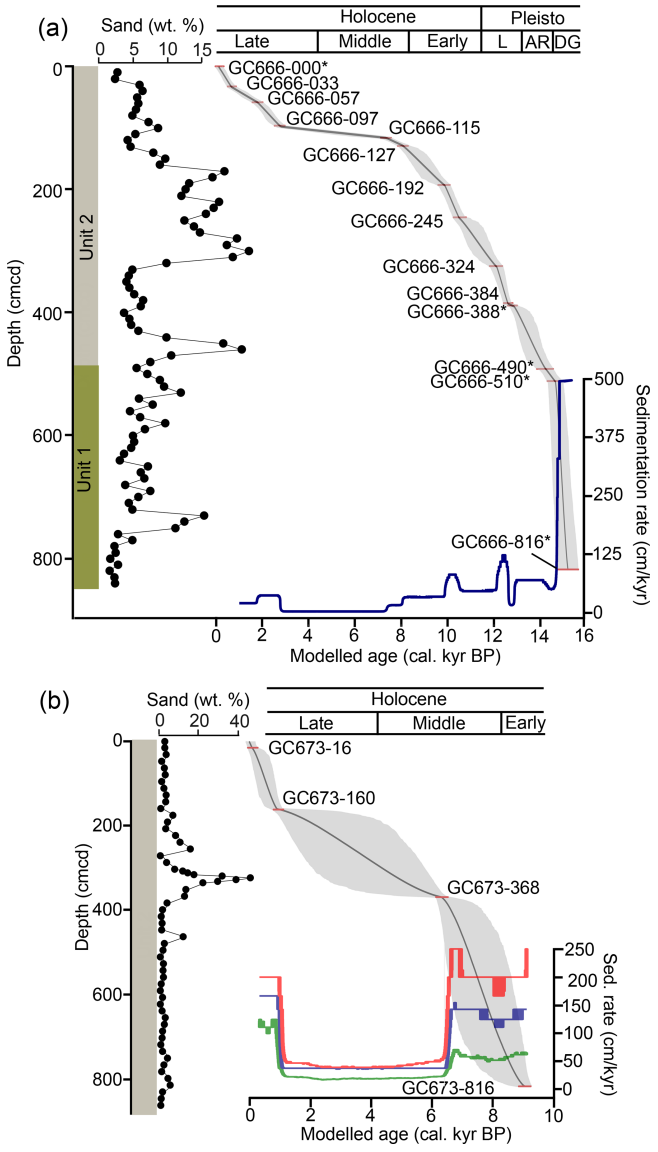

Figure 2. Age–depth models from GC666 **(a)** and GC673 **(b)** calculated using BChron, a Bayesian chronology model, with sedimentation rates. Unit 1 in GC666 represents late Pleistocene laminated diatomaceous mud, and Unit 2 represents homogeneous sandy diatomaceous mud. The entirety of GC672 is homogeneous sandy diatomaceous mud. Pleisto is for Pleistocene; DG is for deglacial; ACR is for Antarctic Cold Reversal; L is for latest Pleistocene. The asterisk (*) indicates samples previously published in Graham et al. (2017).

2.3 Foraminiferal preparation

A total of 89 samples from GC666 and 79 samples from GC673 were analysed for benthic foraminiferal assemblages. Samples were selected based on predicted ages to ensure that the temporal resolution between specimens was as similar as possible, aiming for a 100-year resolution.

Approximately half of the freeze-dried material was processed for micropalaeontology. Samples were washed with deionised water over a 63 µm sieve. The > 63 µm fraction was then dried at 40 °C in a porcelain crucible over 24 h. After drying, the material was viewed under a microscope to decide if it needed to be rewashed. If so, the material was reprocessed using the same methodology. Once the sample was clear of clay residue, it was weighed and placed into a labelled 10 mL plastic vial.

About half of the freeze-dried material was sieved for micropalaeontology. All foraminifera from the > 63 µm fraction were counted and identified using the species concepts developed in Dejardin et al. (2018). To generate statistically significant assemblage data, in line with standard practice, we aimed to count a target minimum of 300 specimens from each sample, but this was not always possible (Fig. 3). The total residue was split in half (to retain some material for other analyses), and the half used for counting was split into three size fractions (> 250 µm, 125 to 250 µm, and 63 to 125 µm) to make the picking easier. All the foraminifera in each size fraction were counted.

2.4 Diversity indices and statistical analysis

Fisher's alpha diversity (Fisher et al., 1943), using the number of foraminiferal species and number of specimens, was calculated using PAST v.4.03 (Hammer, 2022). All the specimens were used to calculate diversity from every analysed sample from both localities. Cluster analysis of the benthic foraminiferal assemblage (BFA) data was carried out in PAST4.03 using absolute abundance data after taxa constituting < 1 % of total counts in all samples in each core were removed. Cluster analysis (UWPGA algorithm; chord similarity matrix) was applied to the benthic foraminiferal data to assess whether statistically significant groups of similar assemblages are present. The detrended correspondence analysis (DCA) module uses the same algorithm as Decorana (Hill and Gauch, 1980), with modifications according to Oksanen and Minchin (1997). The DCA analysis of the BFA data was undertaken in PAST v.4.03, using the absolute abundance data after taxa which were < 1 % of total counts in all samples were removed. DCA is used in preference to the standard correspondence analysis as it removes the "horseshoe effect" that commonly occurs.

2.5 Geochemistry

GC666 was sampled to assess organic carbon content at 4 cm resolution within the upper 515 cmcd and at 64 cm resolution between 515 to 816 cmcd; GC673 was sampled for organic geochemistry at 16 cm resolution throughout. To prepare the samples for percentage organic carbon (% C_{org}) analysis, approximately 500 mg of sample was added to 5 % HCl to remove the carbonate. The samples were then rinsed in deionised water, dried at 40 °C, and then ground to a

fine powder and homogenised before being transferred to a vial. Samples were analysed using a VG Optima dual-inlet mass spectrometer, following combustion using a Costech ECS 4010 elemental analyser at 1400 °C, at the NERC Isotope Geosciences Laboratory, British Geological Survey (BGS), Keyworth, UK. Isotope values were calculated to the VPDB (Vienna Pee Dee Belemnite) scale in parts per thousand using within-run laboratory standards calibrated to international National Bureau of Standards (NBS) standards. The $\%\,C_{org}$ is reported as the organic carbon accumulation rate (C_{org} AR ($g\,kyr^{-1}$)), which was calculated using the following Eq. (1):

$$C_{org}\ AR = (\%\,C_{org}/100) \times \text{mass accumulation rate (MAR)}. \quad (1)$$

A total of 65 samples from cores GC666 and 28 samples from GC673 were analysed for biogenic opal/silica (BSi) at the University of Nottingham, Nottingham, UK, following the method modified by Conley and Schelske (2001) from that of Demaster (1981). For each sample, 30 mg of freeze-dried sediment was placed into 125 mL flat-bottomed polypropylene bottles, 40 mL of 1 % $NaCO_3$ solution was added to the bottles, and the bottles were placed in a heating bath at 85 °C and agitated every 30 min. After 5 h, 1 mL of liquid was pipetted into centrifuge tubes containing 9 mL of 0.021 N HCl; this sub-sampling was repeated after 6 and 7 h. The biogenic opal accumulation rate (BSi AR; reported to 2SF) was calculated from the biogenic opal weight %.

A linear least squares regression analysis was applied to the increase in BSi, extracted versus time, over the three sub-samples for each sample (considering the various dilution steps and the amount of sediment used). This was then extrapolated to the intercept, giving the BSi weight percentage (wt %) for each sample, to correct for any mineral silicates (SI) that may have also been dissolved during the digestion process. Where there was no increasing trend, the mean of the three sub-samples was used; the mean of the three sub-samples was also used where the BSi wt % was greater than 10 % (Conley and Schelske, 2001). These values were then converted into an accumulation rate using Eq. (2):

$$BSi\ AR = (\%\,BSi/100) \times MAR. \quad (2)$$

Oxygen ($\delta^{18}O$) and carbon ($\delta^{13}C$) stable isotope values were measured from calcareous benthic foraminifera (*Cassidulinoides parkerianus*) using a target weight of > 100 µg. One to four specimens of *C. parkerianus* from 73 samples from GC666 and 35 samples from GC673 were measured. All isotope measurements were performed at the NERC Isotope Geosciences Laboratory using an IsoPrime 100 dual-inlet mass spectrometer. Isotope values were calculated to the VPDB using a within-run laboratory standard (KCM).

3 Results

3.1 Age–depth models

GC666 spans from the late deglacial to late Holocene (ca. 15.2–0.1 cal. kyr BP) based on 14 radiocarbon dates (Table 2; Fig. 2). The sedimentation rate throughout the GC666 core was found to be highly variable, spanning 3 orders of magnitude, and particularly high in the deglacial (Fig. 2). The boundary between Unit 1 (laminae and deglacial) and Unit 2 (diatomaceous mud) is equivalent to approximately 14 cal. kyr BP and broadly coincident with the recognised ACR (Putnam et al., 2010). Unit 2 has much lower sedimentation rates during the early Holocene (averaging ca. 47 $cm\,kyr^{-1}$), before dropping further during the mid-Holocene, which has the lowest sedimentation rates (averaging ca. 7.5 cm kyr). Sediment accumulation rates remain low (ca. 4 to 11 cm kyr) until ca. 2.8 cal. kyr BP, before increasing to ca. 30 cm kyr (Fig. 2).

By contrast, GC673 spans the early Holocene to the late Holocene (ca. 9.5 to 0.3 cal. kyr BP) based on four radiocarbon dates (Table 2). The sedimentation rates in GC673 throughout the Holocene are higher in GC673 than those in GC666, although the overall shape of the profile has similarities with lower mid-Holocene rates at both sites followed by increases into the late Holocene (Fig. 2).

3.2 Benthic foraminifera

In GC666, a total of 26 891 benthic foraminiferal specimens from 47 taxa were identified in the 89 samples, and 185 specimens of the planktonic taxa *Neogloboquadrina pachyderma* were identified in 37 samples. There were 300 or more benthic specimens present in 41 samples, and a further 26 samples with lower-foraminifera concentrations contained 100–300 specimens.

In GC673, a total of 24 229 benthic foraminiferal specimens from 45 taxa of benthic foraminifera were identified in 79 samples. In addition, 65 planktonic foraminifera, all belonging to *Neogloboquadrina pachyderma*, were identified from 24 samples. There were 300 or more benthic specimens present in 32 samples, and a further 38 samples contained 100–300 specimens due to lower-foraminifera concentrations. The foraminiferal taxa reported in this study are in agreement with assemblages reported by Majewski et al. (2023), though the cores from this study represent a more distal setting. Taxonomic details and images of most species can be found in Dejardin et al. (2018).

3.2.1 Diversity

In GC666, Fisher's alpha and species diversity increase from the deglacial and into the early Holocene (ca. 15.1 to 8.5 cal. kyr BP), reaching a peak of 22 species at ca. 8.5 cal. kyr BP, before decreasing to 2 species during the

Table 2. Radiocarbon age determinations for GC666 and GC673. A reservoir effect of 433 ± 41 years was applied based on live-stain benthic foraminifera from Dejardin (2017). Minimum and maximum calibrated ages are reported to 2 standard deviations. UnID indicates unidentified samples.

Sample details		Conventional ages		Calibrated ages (Marine_20)		
Depth (cmcd)	Carbonate source	^{14}C Age (year)	Error (± year)	Min (cal. yr BP)	Max (cal. yr BP)	Median (cal. yr BP)
GC666						
0[a]	Benthic forams	1097	43	5	280	115
33[b]	Benthic forams	1715	30	552	863	690
57[b]	Benthic forams	2775	35	1591	1967	1783
97[b]	Benthic forams	3590	35	2669	3055	2833
115[b]	Benthic forams	7520	50	7100	7522	7345
127[b]	Benthic forams	8180	60	7858	8258	8049
192[b]	Benthic forams	9750	50	9631	10120	9896.5
245[b]	Benthic forams	10160	50	10286	10787	10516
324[b]	Benthic forams	11370	60	11875	12400	12136
384[b]	Benthic forams	11780	60	12473	12776	12640
388[a]	Gastropod	11856	65	12710	13066	12872.5
490[a]	Benthic forams	13291	74	14006	14574	14262.5
510[a]	Shell fragments	13301	135	14367	14982	14683
815[a]	Benthic forams	13572	211	14804	15669.5	15212.5
GC673						
16[b]	Benthic forams	1120	37	10	291	138
160[b]	Benthic forams	1990	37	780	1161	967
368[b]	Benthic forams	6567	38	6238	7160	6450
816[b]	Bivalve (UnID)	9072	39	8869	9308	9090.5

[a] Samples previously published in Graham et al. (2017); [b] New samples.

mid–late Holocene (ca. 6.1 to 3.6 cal. kyr BP) (Fig. 3). Diversity indices increase through the late Holocene (ca. 3.1 cal. kyr BP to recent). Diversity indices remain more stable throughout GC673 compared to GC666 (Fig. 3), whereby the mid–late Holocene period of low diversity recorded in GC666 is not present in GC673.

3.2.2 Benthic foraminiferal assemblages (BFAs)

The same BFAs (*Fursenkoina* assemblage, *Miliammina* assemblage, and *Cassidulinoides* assemblage) are reported from both gravity cores based on cluster analysis and DCA (Figs. 3, 4, S1, and S2). Specifically, cluster analysis was used as the primary way to define the major assemblages, using the highest-level branches for each site (which produced three assemblage for each site). DCA was used as a second statistical measure to confirm these groupings and the species most closely associated with them (Fig. 4). In GC666, the *Fursenkoina* assemblage is dominant through the deglacial and into the early Holocene (ca. 15.1–10.7 cal. kyr BP), with intermittent horizons of the *Miliammina* assemblage occasionally prevalent. The *Fursenkoina* assemblage in GC666 is diverse (mean Fisher's alpha = 2.2 ± 0.8) but dominated by *F. fusiformis*, which comprises an average of 68.1 ± 13.3 % of the assemblage (mean dominance = 0.5 ± 0.2). Other species in the assemblage include *M. earlandi* (8.2 ± 8.5 %), *C. parkerianus* (4.9 ± 3.6 %), *A. echolsi* (4.8 ± 4.2 %), and *C. porrectus* (4.7 ± 4.2 %), in addition to smaller abundances of *Globocassidulina crassa rossensis* (2.6 ± 2.2 %), and *Nonionella iridea* (2.4 ± 2.3 %). The *Miliammina* assemblage occurs throughout the core and is the dominant assemblage during the mid–late Holocene (ca. 6.6–0.8 cal. kyr BP). The diversity of the *Miliammina* assemblage is low (mean Fisher's alpha = 1.47 ± 1.15), becoming mono-specific at times, combined with high dominance (mean dominance = 0.55 ± 0.24). The dominant species in the *Miliammina* assemblage are *M. earlandi* (66.6 ± 22.8 %) and *M. lata* (10.9 ± 12.4 %). The *Cassidulinoides* assemblage is occasionally the dominant assemblage through the Holocene in both cores and appears to have the highest diversity (mean Fisher's alpha = 3.9 ± 1.1). The major components of the *Cassidulinoides* assemblage in GC666 are *M. earlandi* (15.7 ± 5.6 %), *C. porrectus* (13.6 ± 6.3 %), *C. parkerianus* (12.7 ± 8.1 %), *A. echolsi* (12.5 ± 4.9 %), and *G. crassa. rossensis* (10.6 ± 11.2 %). Subsidiary species include

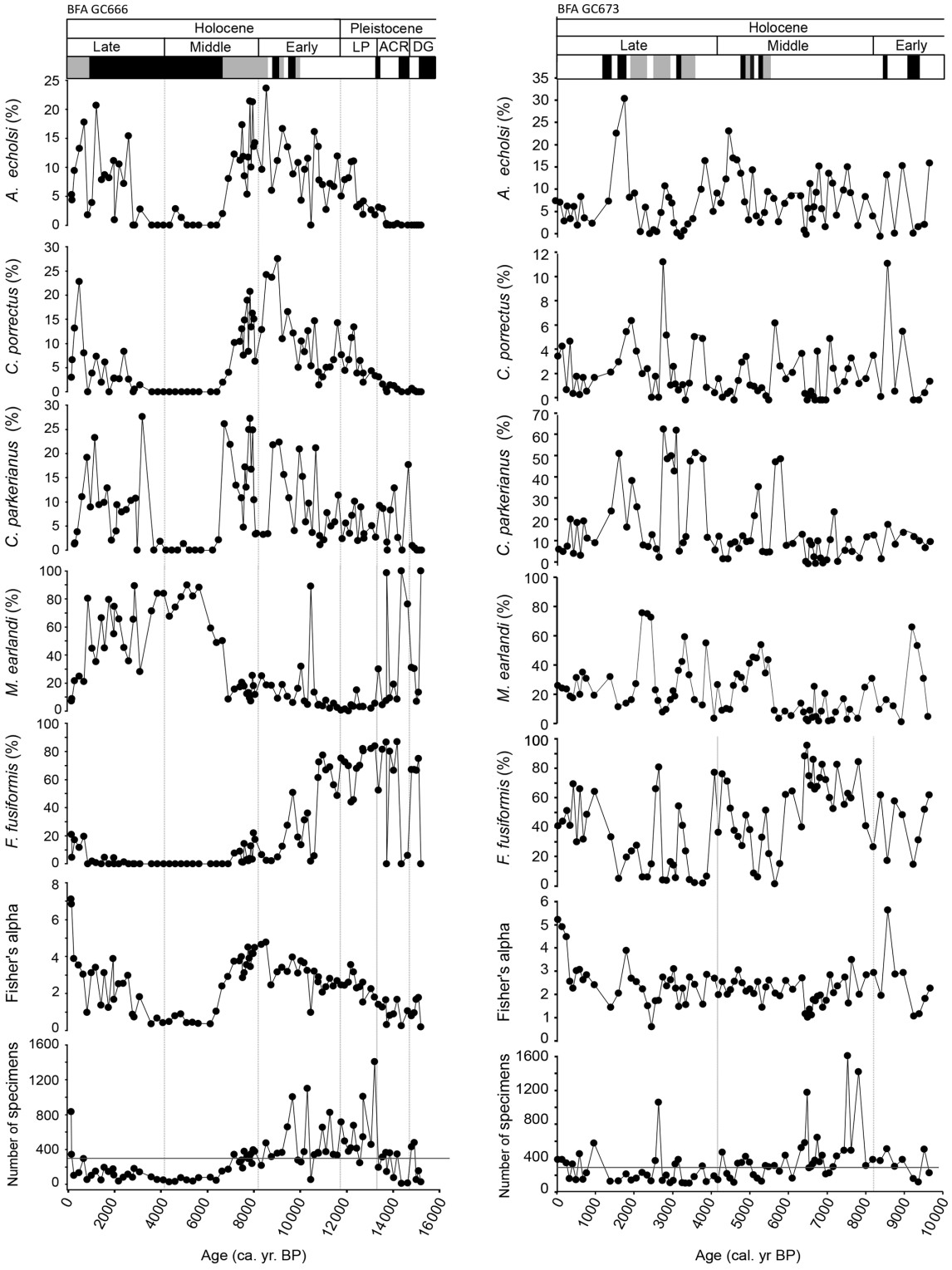

Figure 3. Foraminiferal assemblage percent data showing common taxa and diversity indices with the corresponding assemblage highlighted. White is the *F. fusiformis* assemblage; black is the *M. earlandi* assemblage; grey is the *C. parkerianus* assemblage. Assemblages are based on results from the cluster analysis and DCA (see Figs. S1 and S2 in the Supplement). The horizontal line across the number of species demarks 300 specimens. DG is for deglacial; ACR is for Antarctic Cold Reversal; LP is for latest Pleistocene.

F. fusiformis (10.9 ± 8.5 %), *Buccella* sp. 1 (5.6 ± 4.1 %;), and *Trifarina earlandi* (7.8 ± 7.2 %).

In GC673, it is the *Fursenkoina* assemblage that dominates much of the Holocene (Fig. 3). The *Fursenkoina* assemblage from GC673 is diverse (mean Fisher's alpha = 2.35 ± 2.85), with the dominant taxa being *F. fusiformis* (61.9 ± 44.8 %), *M. earlandi* (14.3 ± 26.7 %), and *C. parkerianus* (7.7 ± 16.2). The *Miliammina* and *Cassidulinoides* assemblages occur intermittently throughout the GC673 with neither becoming the dominant assemblage for a sustained length of time. The *Miliammina* assemblage is more diverse in GC673 compared to GC666 (mean Fisher's alpha = 1.68 ± 1.1), with the dominant taxa being *M. earlandi* (59.4 ± 14 %), *F. fusiformis* (15.2 ± 9.3 %), and *C. parkerianus* (10.9 ± 4.9 %). The *Cassidulinoides* assemblage is less diverse in GC673 (mean Fisher's alpha = 2.39 ± 0.7 %), with the main components being *C. parkerianus* (50.7 ± 14.1 %), *Buccella* sp. A (11.9 ± 11.9), and *A. echolsi* (7.4 ± 15.2 %) with subsidiary species including *F. fusiformis* (6.7 ± 16.95 %) and *C. porrectus* (4.2 ± 3.4 %). The ecological requirements for the dominant species and the results of the DCA are provided in the Supplement.

3.3 Geochemistry

In GC666 (Fig. 5), C_{org} AR values range from 0.22 to 26.7 g cm^{-2} kyr^{-1}, with the highest values recorded at ca. 14.9 cal. kyr BP. BSi AR ranges across several orders of magnitude from 1.3 to 450 g cm^{-2} kyr^{-1}, with the highest value also recorded at ca. 15 cal. kyr BP. Benthic foraminiferal δ^{13}C values throughout GC666 range from −7.9 ‰ to +1.1 ‰. Values below −1 ‰ only occur during the deglacial to early Holocene (ca. 14.7 and 10.2 cal. kyr BP) and at ca. 3.8 cal. kyr BP. The δ^{13}C values between 14.7 and 10.2 cal. kyr BP fluctuate widely between −7.9 ‰ and 0 ‰; the foraminifera analysed from this period appear to have been diagenetically altered. They are yellow/brown in colour compared to the pristine white or glassy specimens and are covered with varying degrees of "sugary" crystal overgrowths. There are no isotope data between ca. 6.3 and 3.1 cal. kyr BP, except for the sample at ca. 3.8 cal. kyr BP, due to the absence of calcareous foraminifera in this part of the core. δ^{18}O values for GC666 range from +3.6 ‰ to +5.7 ‰, although the peak value, at ca. 14.5 cal. kyr BP may be an outlier as it is > 0.5 ‰ higher than the surrounding values. The overall curve/shift in benthic δ^{18}O values follows the deglacial trend seen in the global deep-ocean composite record "Prob-stack" (Ahn et al., 2017; see Lisiecki and Raymo, 2005) with an offset of ca. +0.5 ‰, suggesting the first-order changes in our record are reflecting shifts in global seawater δ^{18}O from a reducing ice volume.

In GC673 (Fig. 5), C_{org} AR values range from 1.5 to 13.5 g cm^{-2} kyr^{-1}, with the highest value recorded at ca. 7.3 cal. kyr BP. The BSi AR values range from 33.6 to 241 g cm^{-2} kyr^{-1}, with the highest value recorded at ca. 9.2 cal. kyr BP. δ^{13}C values range from −6.3 ‰ to +0.7 ‰. Negative δ^{13}C values only occur between ca. 9.2 and 5.9 cal. kyr BP and are generally associated with foraminifera that appear to have been diagenetically altered, as seen in GC666. After ca. 5.9 cal. kyr BP there is little variation in δ^{13}C (mean = +0.45 ± 0.15 ‰). Benthic δ^{18}O values range from +3.4 ‰ to +4.1 ‰ and broadly follow the trend seen in the Prob-stack with and offset of ca. +0.6 ‰.

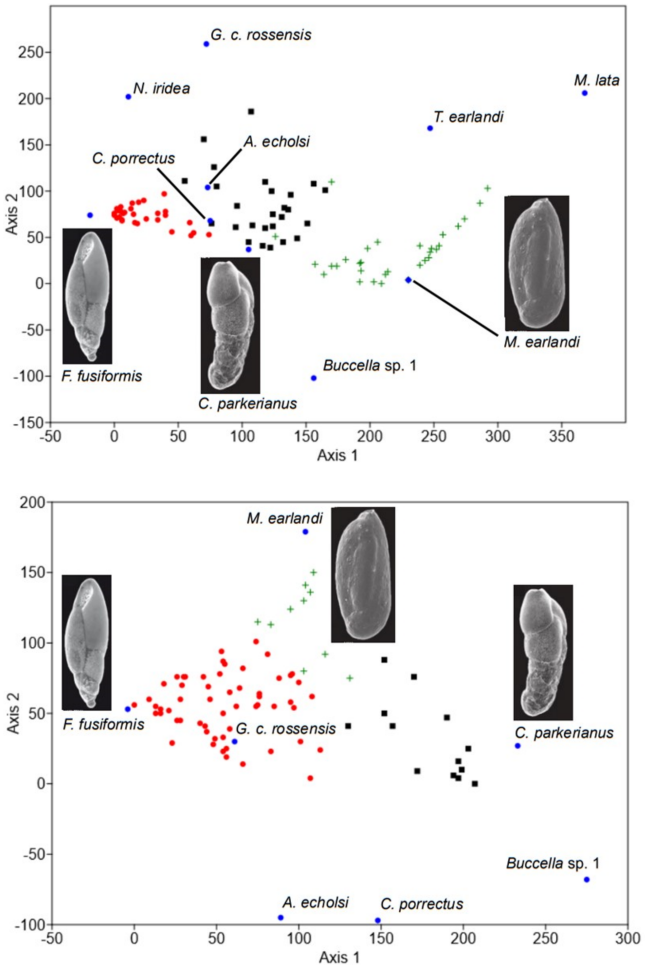

Figure 4. Detrended correspondence analysis (DCA) on benthic foraminiferal data from GC666 (top panel) and GC673 (bottom panel). The figure shows how the three assemblages (as defined using cluster analysis; see Sect. 2) are grouped together based on their species compositions and which species are associated with assemblage. Symbols show the three assemblages: red circles are for the *F. fusiformis* assemblage; black squares are for the *C. parkerianus* assemblage; green crosses are for the *M. earlandi* assemblage. SEM photographs are taken from Dejardin et al. (2018).

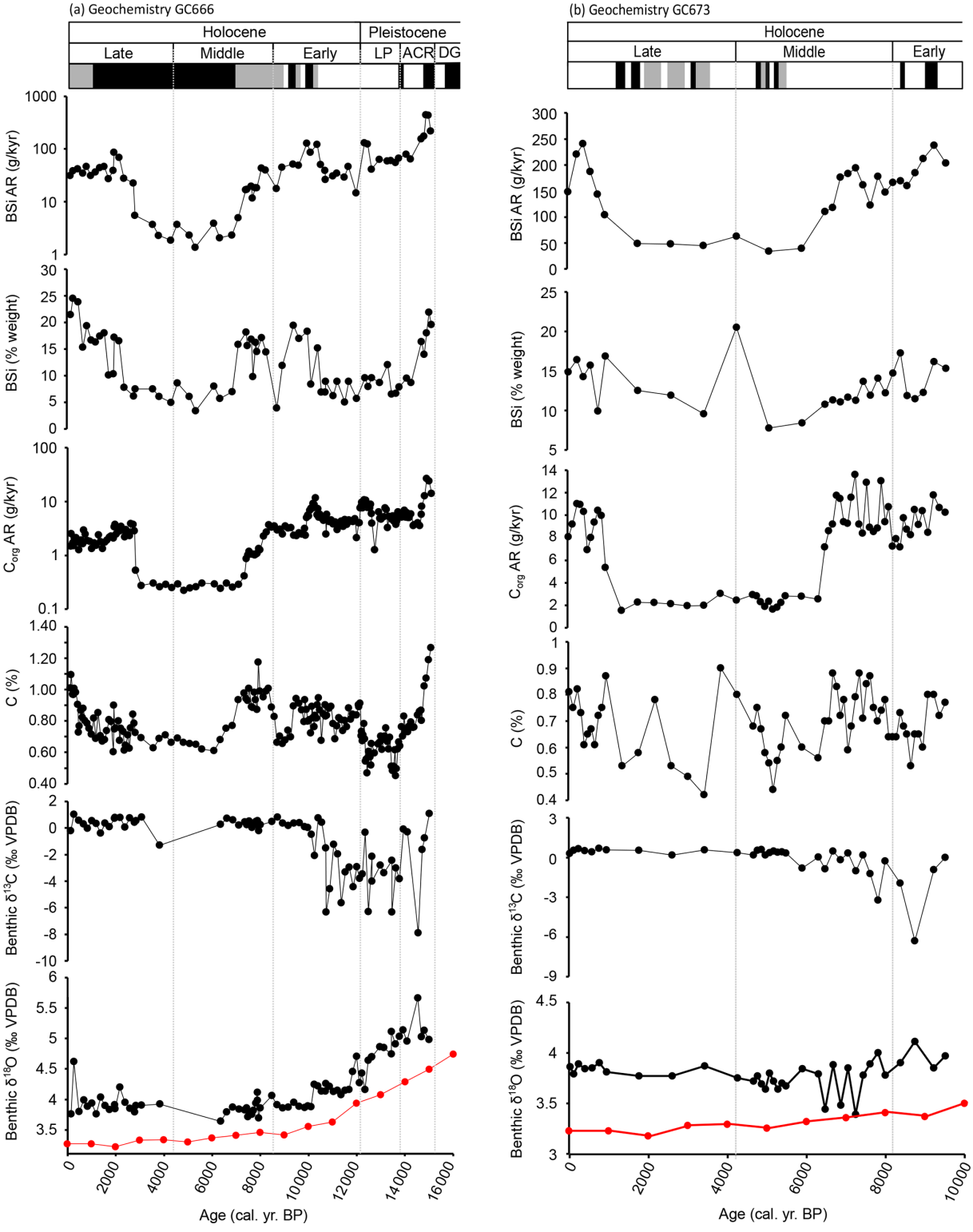

Figure 5. Geochemical analyses on sediment and foraminifera from cores GC666 **(a)** and GC673 **(b)**, with the corresponding assemblage highlighted with white for the *F. fusiformis* assemblage, black for the *M. earlandi* assemblage, and grey for the *C. parkerianus* assemblage. Red δ^{18}O data points are from the global composite LR04 stack (Lisiecki and Raymo, 2005). DG is for deglacial; ACR is for Antarctic Cold Reversal; LP is for latest Pleistocene.

4 Discussion

4.1 Preservation and causes of carbonate dissolution

The preservation of benthic foraminifera is mostly very good throughout both cores, but there is evidence of diagenetic alteration and several dissolution horizons in both GC666 and CGC673 (Fig. 6). Constraining the degree of dissolution is not straightforward, as lower relative abundance of calcareous foraminifera compared with agglutinated species could be a result of palaeoenvironmental change such as colder saline shelf water (e.g. Peck et al., 2015). We estimate samples where either the dominance of agglutinated species is very high (> 50 % of total assemblage) or the dissolution-resistant *M. earlandi* (see Ishman and Sperling, 2002) is predominant (above 70 %) as likely dissolution horizons (shaded bars in Fig. 6). The interpreted dissolution intervals between ca. 15.1 and 10.4 cal. kyr BP in GC666 co-occur with high carbon flux (Figs. 5, 6), evidenced by the high C_{org} AR and % C_{org} and negative $\delta^{13}C$ values. This relationship indicates the possible corrosivity of the pore- and bottom-water chemistry which would be unfavourable for the preservation of thin-walled species such as *F. fusiformis*. Species like *M. earlandi*, by comparison, have a thick, agglutinated test that is less affected by increased corrosivity, which could lead to this taxon becoming dominant due to preservation biases (Majewski and Anderson, 2009). The elimination of calcareous species, even at shallow depths, due to dissolution is also observed by other authors (e.g. Majewski et al., 2016) in the Southern Ocean.

Within GC666, the interval prior to ca. 14 cal. kyr BP likely represents a period of high productivity, as evidenced by elevated sedimentation rates (laminated unit), high C % and BSi accumulation (Fig. 5), and abundant *F. fusiformis* (Figs. 3, 6). These observations, along with anomalously negative benthic $\delta^{13}C$ values (Figs. 5, 6), indicate that the dissolution levels may have been caused by bottom-water corrosion and/or diagenetic alteration due to the high flux of organic matter to the seafloor leading to elevated CO_2 and the acidification of porewaters. In a study of sediment cores dating from the present to the last deglacial from Maxwell Bay on the Antarctic Peninsula, Li et al. (2000) considered a high relative abundance of agglutinated benthic foraminifera to be a potential proxy for carbonate dissolution. These diagenetically altered samples of porcelaneous foraminifera exhibit orange discolouration and sugar-like overgrowth covering the tests during the Pleistocene and early Holocene in the study by Li et al. (2000) (compare Fig. 3 in Li et al., 2000, to scanning electron microscopy (SEM) images presented in Fig. 6 in this study) and are similar in appearance to the methane-derived authigenic carbonate reported elsewhere (e.g. Svalbard, Schneider et al., 2017; Bering Sea, Detlef et al., 2020). Possible precipitation of authigenic carbonate in the laminated Unit 1 is thought to be the result of methane produced deeper in the core (Meisel et al., 2014). Pohlman et al. (2013) found that authigenic carbonate resulted in ^{14}C ages from foraminifera that were 50 to 400 years older than their true ages. The presence of inorganic carbonates in GC666 being derived from methane is supported by the identification of widespread methane seepage over the South Georgia shelf, including Royal Bay (Römer et al., 2014). Rapid sedimentation, such as that recorded in Unit 1, favours biogenic methane production (e.g. Hein et al., 1979), and methane may have continued to form within Unit 1 while the overlying sediments were deposited, migrating vertically and causing diagenetic alteration of foraminifera.

Benthic foraminifera after ca. 10.1 cal. kyr BP (211 cmcd) in GC666 and ca. 9.2 cal kyr BP (832 cmcd) in GC673 do not appear to have been altered by inorganic carbonate precipitation from methane formation. The cause of the sporadic mid- and late-Holocene dissolution in GC666 and GC673 may, alternatively, be due to lower sedimentation rates leading to longer exposure times of the foraminifera to mildly corrosive bottom waters before burial. This may account for why GC666 has much more dissolution than GC673, as it has lower sedimentation rates (Figs. 2, 6). The fewer dissolution horizons in GC673 imply that the *M. earlandi* assemblage in this core may be used to infer palaeoenvironmental change rather than being primarily an artefact of dissolution (as in GC666).

The increase in diversity in the youngest part of GC673 and GC666 may be due to enhanced preservation, as most of the agglutinated taxa (*Haplophragmoides quadratus*, *Labrospira* sp., *Glaphyrammina rostrata*, *Pseudobolivina antarctica*, *Pseudotrochammina* sp., and *Textularia earlandi*) are only found in the youngest sediments in GC666. This is likely because the organic cement secreted by these foraminifera usually disintegrates soon after death (Mackensen et al., 1995), in contrast to *Miliammina*, which has siliceous cement (Dejardin et al., 2018) and is more robust.

4.2 Palaeoenvironmental change

4.2.1 Deglacial (15.2 to 14.7 cal. kyr BP)

Following the LGM (26.5 to 19.0 cal. kyr BP), increasing temperatures, primarily driven by changes in insolation, resulted in global deglaciation between 19 and 11 cal. kyr BP (Clark et al., 2004, 2012). The timing of deglaciation varies between different regions and may be as late as 14.5 cal. kyr BP in Antarctica (Clark et al., 2009). The timing of deglaciation in South Georgia is subject to much debate, linked to uncertainties in the extent of the island's LGM ice sheet (see Bentley et al., 2007; Barnes et al., 2016). Glacial sediments recovered from Little Jason Lagoon may correspond to an ice dome that covered Lewin Peninsula and had retreated from lower elevations around 16 ± 1.5 cal. kyr BP (Berg et al., 2019). Although the onset of deglaciation was not captured in the GC666 record, the later stages of deglaciation are recorded at the bottom of the

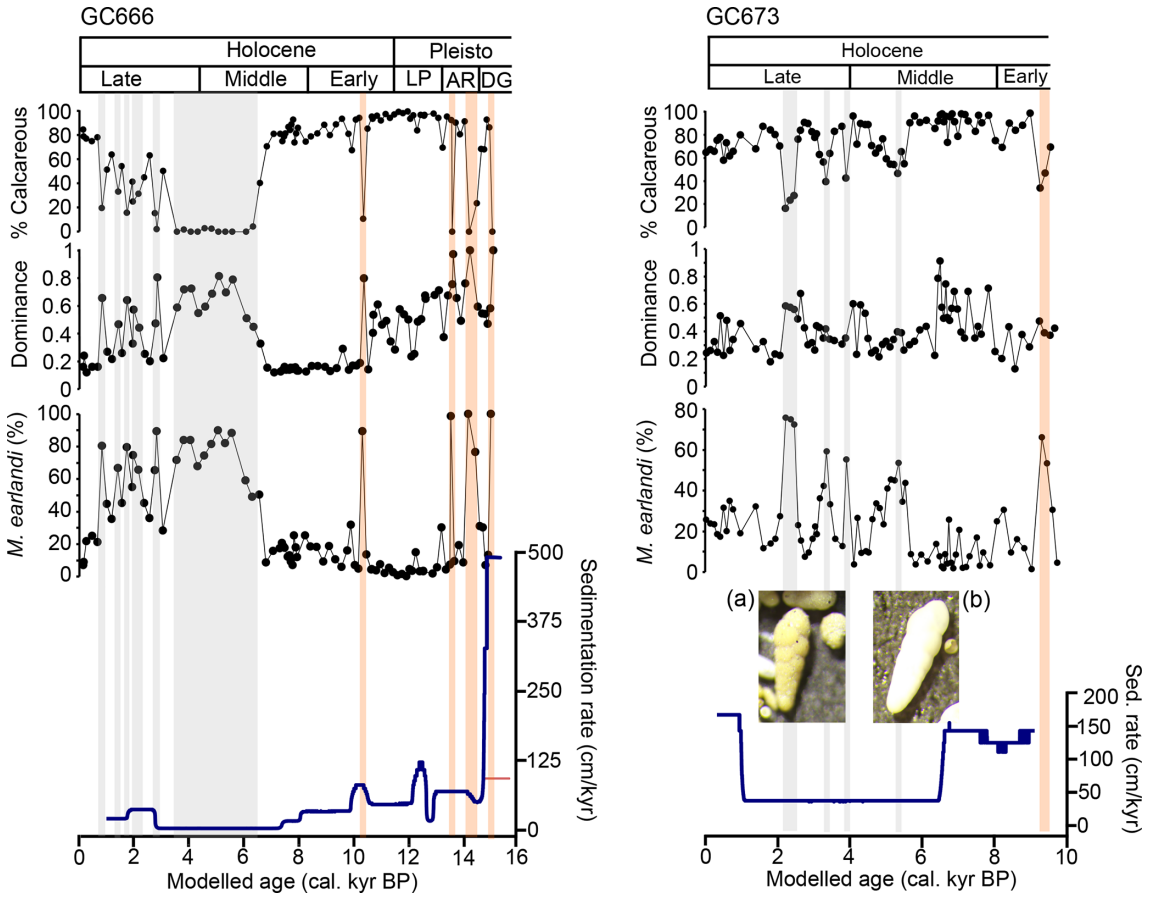

Figure 6. Identification of possible dissolution horizons from GC666 and GC673 as defined where dominance values are above 0.6 and relative abundance of *M. earlandi* is above 70 %. **(a)** *C. parkerianus* specimen from a dissolution horizon (sample GC673; 832 cm). **(b)** *C. parkerianus* specimen from outside a dissolution horizon (sample GC673; 160 cm). DG is for deglacial; ACR is for Antarctic Cold Reversal; LP is for latest Pleistocene. Grey is for likely dissolution caused by the low sedimentation rate; orange is for likely dissolution resulting from high productivity.

core in the thick basal package of laminated sediment (816 to 510 cmcd; ca. 15.2 to 14.7 cal. kyr BP) which was deposited much more rapidly than the remaining sediments with average sedimentation rates of ca. 500 cm kyr^{-1} (Fig. 2). One possible explanation for the high sedimentation rates is enhanced biological productivity during the transition out of the last glacial stage (a view also supported in Graham et al., 2017), which is also reflected in the productivity proxies (*F. fusiformis*, BSi AR, C_{org} AR, and % C_{org}; Figs. 3, 5, 7).

The preservation of laminae in GC666 during the late deglacial (15.2 to 14.7 cal. kyr BP) indicates an absence of benthic bioturbation which may result from anoxic conditions at the sediment–water interface (Peck et al., 2015) or from diatom mats that overwhelm the benthos in otherwise oxic bottom waters (Pike and Kemp, 1999). Anoxia could have developed as a result of high productivity and organic carbon flux in the overlying water column, likely in association with ice-proximal conditions (e.g. Ishman and Sperling, 2002; Majewski and Anderson, 2009; Kilfeather et al., 2011). This interpretation is supported by the relatively low diversity of benthic foraminifera; the dominance of *Miliammina earlandi* associated with organic-rich diatomaceous sediments (Majewski et al., 2016); and *Fursenkoina fusiformis* associated with sediments rich in organic matter (Ishman and Domack, 1994; Majewski et al., 2016), high productivity, and carbon flux (Ishman and Sperling, 2002; Peck et al., 2015; Majewski et al., 2016). Alve (1991) reported that *F. fusiformis* dominated the most oxygen-deficient area of the Drammensfjord (Norway), where oxygen values are less than 1 mL L^{-1}, and it was the first species to recolonise the formerly anoxic environment in Drammensfjord (Alve, 1995). Furthermore, the high BSi AR, C_{org} AR, and % C_{org} (Figs. 5, 7) values all suggest that GC666's late deglacial was a period of very high productivity. The extremely high accumulation rate of biogenic silica (Fig. 5) shows that diatom productivity and export was especially high during this period. Where assemblages dominated by *F. fusiformis* are found in recent surface sediments from coastal West Antarctica, they are as-

sociated with intense diatom blooms and periods of high terrigenous sedimentation in glacier-proximal settings (Majewski et al., 2016), and we postulate similar conditions adjacent to South Georgia during the late deglacial. In this setting, sedimentation rates were strongly linked to the pattern of ice retreat. Accordingly, if we use the timing of the major shift in sedimentation as an indicator for glacier retreat, then 14.7 cal. kyr BP (revised from the 14 cal. kyr BP as suggested by Graham et al., 2017) provides a probable minimum age on ice recession from near the vicinity of GC666 in the outer Royal Bay trough.

4.2.2 The ACR and latest Pleistocene (14.7 to 11.7 cal. kyr BP)

The ACR is well documented across the region, occurring between ca. 14.7 and 13 cal. kyr BP (Pedro et al., 2016), and is characterised by cooler temperatures in Antarctica and the advancement of Antarctic (Mulvaney et al., 2012; Xiao et al., 2016) and South American (e.g. Menounos et al., 2013) glaciers. In South Georgia, the ACR has been identified in sediment cores from Little Jason Lagoon indicative of glacial advance (Berg et al., 2019). Cooling during the ACR may have been caused in part by a northward migration in the SWWs to the latitude of South Georgia (Fletcher et al., 2021), which could have altered the precipitation on South Georgia. During the ACR, evidence from seabed landforms and terrestrial sediments suggests that there was a major glacier readvance into Cumberland East Bay (Graham et al., 2017) and perhaps Stromness Harbour (Bentley et al., 2007). A study of lake sediments adjacent to Cumberland Bay fjord revealed that climate cooled during an interval between 14.8 and 14.2 cal. kyr BP, coincident with the ACR (Rosqvist et al., 1999).

The termination of the laminated sequences in GC666 at ca. 14.7 cal. kyr BP approximately coincides with the onset of the ACR, within the uncertainty associated with our age model, and is associated with an increase in the sand content of the sediments from 5 % BP to 10 % BP (Fig. 2). Cooler climates brought on by the ACR provided favourable conditions for glacier advance, which is thought to have been restricted to the fjords with a glacial advance of at least 8 km in Cumberland Bay (Graham et al., 2017). Because the glacial advancement only occurred within the fjords, we do not expect to see a major increase in productivity in the outer (mid-shelf) part of the Royal Bay trough. This interpretation is supported by the BFA regarding the appearance of *Cassidulinoides parkerianus* (Fig. 7), a taxon that is indicative of nearshore glacial conditions (Rodrigues et al., 2010; Majewski et al., 2012) with high freshwater input from melting glaciers (Rodrigues et al., 2010). The extent of this productivity increase caused by the ACR was not as extreme as those seen during the late deglacial (ca. 500 cm kyr^{-1}); hence, there was no return to laminated sedimentation. Instead, productivity in the mid-South Georgia shelf remained moderately high (ca. 60 cm kyr^{-1}) during the ACR, as indicated by no significant change in the BFA (Figs. 3, 7).

Through the latter part of the ACR into the latest Pleistocene, the BFA became more species-rich and diverse, indicating a less stressed and possibly more oxic environment (Fig. 3). Glaciers may have become more distal as temperatures increased, and this putative melting ice could account for the almost doubled sedimentation rate between ca. 12.6 and 12.1 cal. kyr BP (Fig. 2). This immediately follows the accepted end of the ACR at 12.8 cal. kyr BP (Putnam et al., 2010) when glaciers retreat to within the fjords and bays (Clapperton et al., 1989; Hodgson et al., 2014b). Melting ice, or increased freshwater runoff (Oksman et al., 2022), could also cause an increase in productivity, as evidenced by an increase in BSi AR and C_{org} AR and a slight increase in diversity (Figs. 3, 5, 6). Furthermore, terminal moraines from many of the fjords around South Georgia have been dated to 12.2 ± 1.5 cal. kyr BP (Bentley et al., 2007), supporting our interpretation that the end of the Pleistocene was a period of retreating glaciers. The only noteworthy change in the BFA within the latest Pleistocene of GC666 was the appearance of *Astrononion echolsi* (Figs. 3, 7), which is an indicator of distal glaciomarine environments (Majewski, 2005, 2010; Majewski et al., 2016) favouring warmer, fresh shelf water (Anderson, 1975; Milam and Anderson, 1981) and well-oxygenated bottom waters (Schmiedl and Leuschner, 2005). At 12.3 cal. kyr BP, there was a rapid increase in *Astrononion echolsi* and *Cassidulinoides porrectus* (sensu Dejardin et al., 2018) (Figs. 3, 7). Both these species are indicative of warm, fresh shelf water with a stable food supply on the Antarctic Peninsula (Majewski et al., 2016), which may have been more analogous to South Georgia during the latest part of the deglacial. A decrease in BSi AR and C_{org} AR within the ACR (Fig. 7) suggests less primary productivity and declining meltwater nutrient input, again supporting the interpretation of near-open-ocean conditions and more distal glaciers.

4.2.3 Early Holocene (11.7 to 8.2 cal. kyr BP)

During the earliest Holocene (11.7 to 10.8 cal. kyr BP) in GC666, the BFA remained dominated by *F. fusiformis*, indicating high organic carbon flux, and diversity remained stable (Figs. 3, 7). The geochemical proxies from GC666 indicate that productivity was slightly lower at the start of the early Holocene than it was during the late Pleistocene and gradually decreased towards ca. 8.2 cal. kyr BP, which spans a time of gradually cooling air mass temperatures over James Ross island (Fig. 7). The early to mid-Holocene captured in GC673, 9.5 to 8.2 cal. kyr BP, indicates higher overall productivity and accumulation rates than at GC666 and variable productivity trends from *F. fusiformis*, BSi AR, and C_{org} AR into the mid-Holocene. The steady decrease in productivity at GC666 may be due to a decrease in terrestrial runoff from Royal Bay as glaciers retreated further into the inner fjords. Due to the GC673 having closer proximity to

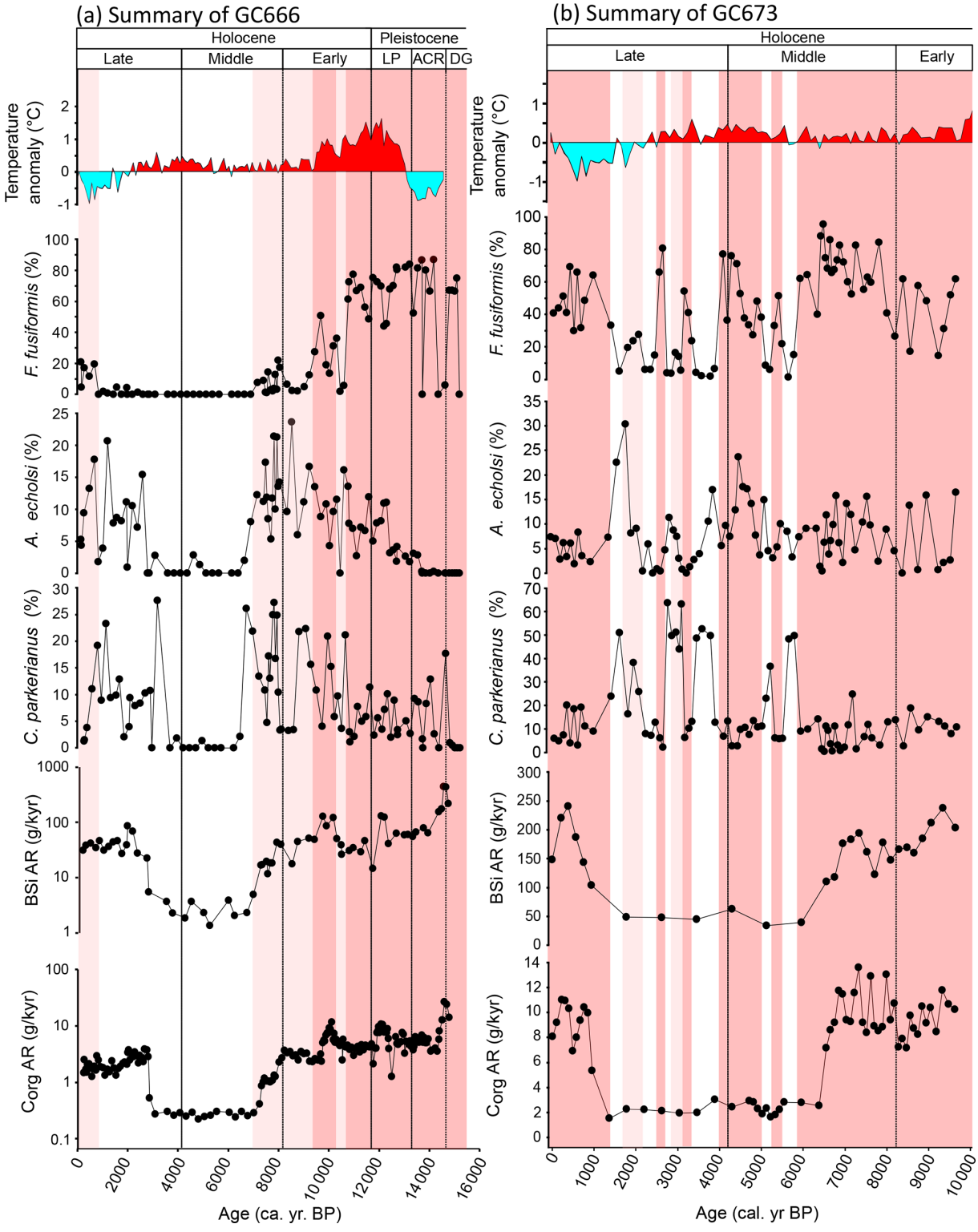

Figure 7. Summary chart of productivity reconstructions from GC666 **(a)** and GC673 **(b)**. Pink bars represent the elevated proportion of *F. fusiformis* and inferred high organic carbon flux. Temperature anomalies are taken from the James Ross island ice core (Mulvaney et al., 2012). DG is for laminated sediments; ACR is for Antarctic Cold Reversal; LP is for latest Pleistocene.

the shoreline, where much higher primary productivity occurs today (Borrione et al., 2014), it would be expected that GC673 would be more influenced by terrestrial runoff than at GC666, and this could account for its later transition into a low-productivity regime (ca. 6.5 cal. kyr BP as opposed to 7.3 cal. kyr BP, Fig. 7). Today, waters of the surrounding Southern Ocean are rich in macronutrients and limited by dissolved iron (Nielsdóttir et al., 2012), and modelling and proxy studies have shown that shallow coastal regions of South Georgia, rather than atmospheric dust, are the most important contributors of marine iron and associated productivity (Borrione et al., 2014). Although other factors could have contributed to Holocene changes in primary productivity on the South Georgia shelf, including changes to the SWWs and position/strength of the Southern Antarctic Circumpolar Current Front (SACCF) (Combes et al., 2023) or iron delivery from icebergs (Ardelan et al., 2010).

The implication of our BFA record is that the glaciers became more distal from ca. 10.7 cal. kyr BP, as evidenced by the collapse in the relative abundance of *F. fusiformis* and the increase in *C. parkerianus, C. porrectus,* and *A. echolsi*, which all imply more open waters with less intense seasonal blooms and associated organic carbon flux (Fig. 7). This reduction in *F. fusiformis* abundance in GC666 approximately corresponds with the onset of the Antarctic early Holocene optimum (11 to 9.5 cal. kyr BP; Berg et al., 2019), where ice core records around Antarctica show widespread warming (Ciais et al., 1992; Masson et al., 2000; Masson-Delmotte et al., 2004). Summer sea surface temperatures from the central Scotia Sea increased between 11 and 9 ka (e.g. Xiao et al., 2016), and sediment cores from the Atlantic sector of the Southern Ocean (Divine et al., 2010) and ice cores from the Antarctic Peninsula (Mulvaney et al., 2012) show elevated temperatures (Fig. 7). Deglaciation of low-altitude sites was apparently well underway in the early Holocene, as evidenced by the onset of biogenic sedimentation in South Georgia lakes and peatlands (van der Putten and Verbruggen, 2005; Berg et al., 2019). These higher temperatures likely supported increasing vegetation and lake productivity in low-altitude areas of South Georgia (e.g. van der Putten et al., 2009; Berg et al., 2019). The Antarctic early-Holocene optimum marks the warmest conditions and strongest sea ice reduction in the Southern Ocean since the last glacial period (Xiao et al., 2016).

Fursenkoina fusiformis remained relatively stable throughout the early Holocene in GC673, implying that glacial nutrient runoff persisted from Cumberland Bay. Both *A. echolsi* and *C. porrectus* are indicative of warm, fresh shelf water (Anderson, 1975; Milam and Anderson, 1981), and *C. parkerianus* lives in environments with high freshwater inputs (Rodrigues et al., 2010). All three taxa can be found in glaciomarine environments (*A. echolsi*, Majewski, 2005, 2010, and Majewski et al., 2016; *C. parkerianus*, Rodrigues et al., 2010, and Majewski et al., 2012; *C. porrectus*, Rodrigues et al., 2010). A high terrestrial input could have been the result of spring/summer melting of glaciers in Cumberland Bay.

4.2.4 Mid-Holocene (8.2 to 4.2 cal. kyr BP)

The mid-Holocene in GC666 is characterised by low BSi AR and C_{org} AR from ca. 7.2 cal. kyr BP, which suggests low productivity (Fig. 7). The BFA is dominated by the agglutinated taxa *Miliammina* spp., which is likely the result of dissolution (Fig. 6). It is possible that the significant decrease in the sedimentation rate allowed porewaters to become more oxidised, leading to an increase in oxic respiration within the sediment and greater carbonate dissolution due to an increase in dissolved inorganic carbon relative to alkalinity. The decrease in sedimentation likely resulted from a reduction in the terrestrial outwash reaching the outer South Georgia shelf, ultimately from reduced glacier extent around Royal Bay. Graham et al. (2017) ruled out glacial erosion at this low sedimentation rate interval due to a lack of sedimentological evidence for ice grounding and suggested that bottom-current winnowing associated with a latitudinal shift in oceanographic fronts may have occurred. However, we propose that it was unlikely to be the result of a major water mass change on the inner shelf, as this is not supported by micropalaeontological or geochemical evidence from GC673.

In contrast to GC666, there is no evidence of extensive dissolution in GC673 during the mid-Holocene, but GC673 did also experienced broadly reduced productivity (lower BSi AR and C_{org} AR) and sediment accumulation rates (Figs. 2, 7). *F. fusiformis* relative abundance decreased at ca. 6.2 cal. kyr BP, followed by several short-term increases (marked as pink bars in Fig. 7) interpreted as brief intervals of increased productivity that did not affect the more distal GC666 site. The peak in *F. fusiformis* at ca. 5.2 to 4.1 cal. kyr BP corresponds with the early-Neoglacial advance hypothesised by Clapperton et al. (1989; Fig. 8). It is important to distinguish that, unlike the enhanced productivity and elevated *F. fusiformis* before ca. 10.9 cal. kyr BP in GC666, which was associated with regional warming and deglaciation, this mid-Holocene peak in *F. fusiformis* in GC673 is associated with smaller-scale glacial readvance and likely cooling. We interpret the elevated productivity as being due to more proximal glaciers delivering more iron-rich terrestrial outwash from seasonal summer melting. In contrast, mid–late-Holocene intervals of low *F. fusiformis* in GC673 coincided with reduced glacial extent around Cumberland Bay and likely warmer conditions overall but with less seasonal meltwater and nutrient delivery.

4.2.5 Late Holocene (4.2 cal. kyr BP to present)

The early part of the late Holocene (ca. 4.2 to 2.8 cal. kyr BP) in GC666 is a continuation of the low sedimentation and low-productivity dissolution zone from the mid-Holocene. Sediments in GC666 from ca. 2.8 cal. kyr BP onwards show

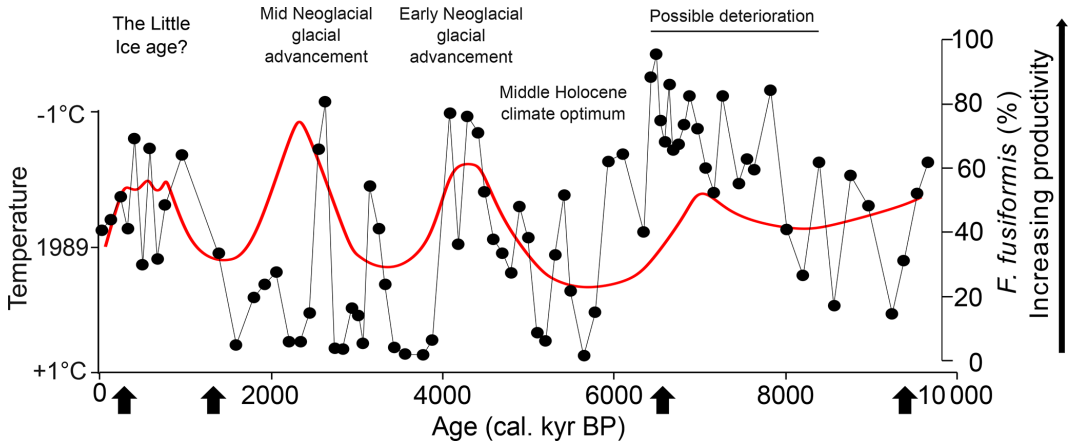

Figure 8. Summary of glacial trends in South Georgia, comparing *F. fusiformis* abundances from GC673 (black data and line) as a proxy for primary productivity with temperature estimates from Clapperton et al. (1989; red line and text). Arrows indicate the position of radiocarbon dates in GC673.

higher sedimentation rates than during the mid-Holocene and evidence of only occasional, short-lived intervals/episodes of dissolution (Fig. 6). The BFA from ca. 2.8 cal. kyr BP has higher diversity than the mid-Holocene but remains dominated by the *M. earlandi* assemblage until ca. 0.8 cal. kyr BP, with the second most dominant taxa being *A. echolsi* (Figs. 3, 7). Both BSi AR and C_{org} AR increase during the late Holocene, returning to early-Holocene values from ca. 2.8 cal. kyr BP onwards (Fig. 7). The rise in productivity and sedimentation rate could be the result of South Georgia becoming wetter (van der Putten et al., 2004) and more glaciated (Clapperton et al., 1989) from 2.6 cal. kyr BP. BFA and productivity proxies from both GC673 and GC666, and palaeotemperature estimates from Annenkov Island (Foster et al., 2016) and James Ross island (Mulvaney et al., 2012), suggests cooler conditions during the late Holocene. In GC673, after continued short-term increases in *F. fusiformis* (pink bars in Fig. 7), the assemblage becomes dominated once again by *F. fusiformis* from ca. 0.9 cal. kyr BP, and productivity proxies increase, similar to the early Holocene, where we interpret more proximal glaciers and associated productivity blooms from seasonal melting and a cooler climate. In GC666, *M. earlandi* was largely replaced by *C. parkerianus* and subsidiary *F. fusiformis* from 1.0 cal. kyr BP, which may indicate seasonal meltwater input and associated nutrients reached further out on the shelf.

Several studies (e.g. Oppedal et al., 2018; Zwier et al., 2021) have suggested colder (summer) conditions and glacial advances on South Georgia starting from ca. 0.9 cal. kyr BP, while Xia et al. (2020) found evidence of more glacial meltwater influence from peat bog cores. The SWWs may have migrated northwards during the late Holocene (e.g. Toggweiler et al., 2006; Anderson et al., 2009; Björck et al., 2012; Browne et al., 2017). Browne et al. (2017) theorised that the SWWs migrated northward to the latitude of South Georgia and strengthened after ca. 1.6 cal. kyr BP, which we suggest may have contributed a forcing mechanism for glacial readvance via the delivery of precipitation. Strother et al. (2015) found increases in non-native and long-distance pollen grains transported from South America, which indicates a stronger SWW around South Georgia which possibly occurred during some "colder" phases of the late Holocene, most notably between ca. 2.2 and 1.7 cal. kyr BP and after 0.7 cal. kyr BP. Van der Bilt (2022) also concluded that colder and wetter conditions on South Georgia during the late Holocene were caused by northward migration and strengthening of the SWWs towards South Georgia. Atmospheric conditions have been suggested as a driver for glacier growth and retreat from modern glaciers (Gordon et al., 2008; Favier et al., 2016).

4.2.6 South Georgia Holocene glacial summary

In an extensive analysis of lake and peat cores and glacial landforms around Cumberland Bay, Holocene glacial fluctuations and palaeoecological changes were reconstructed using terrestrial pollen to present evidence of several glacial advances and retreats since the late deglacial (Clapperton et al., 1989; van der Putten et al., 2004; Foster et al., 2016; Berg et al., 2019). Despite uncertainties with age models from each study, we find broad agreement that times of increased productivity (dominant *F. fusiformis*) in GC673 correspond with the interpretation of cool intervals around Cumberland Bay (Fig. 8).

The earliest part of the GC673 record, before ca. 8 cal. kyr BP, coincided with high productivity at GC666 site. This was unlikely due to a closer shoreline proximity from lower sea levels, which may have only shifted the coastline ca. 15 m lower than present at 9 cal. kyr BP (Barlow et al., 2016), and instead from glaciers extending/remaining beyond the fjords/onto the continental shelf in close proximity to sites GC673 and GC666. From ca. 8 cal. kyr BP onwards,

our records appear to support the interpretation from Clapperton et al. (1989) of a cooler phase (climate "deterioration") until ca. 6.4 cal. kyr BP, followed by a mid-Holocene warming (climatic "optimum") until ca. 5 kyr BP, and cooling centred around 4.2 cal. kyr BP (early Neoglacial). Interestingly, where Clapperton et al. (1989) interpret one subsequent cooling episode at 2.5 kyr BP ("mid-Neoglacial"), we find evidence for two high productivity and inferred cooling episodes at ca 3.2 cal. kyr BP and 2.6 cal. kyr BP within a background of interpreted relative glacial retreat and warmth, although we note that our dating in this interval of the core is less certain as it is farthest from the dated horizons (black arrows in Fig. 8). Clapperton et al. (1989), Berg et al. (2019), and our new data from GC673 show apparent glacial advance during the late Holocene from ca. 0.9 cal. kyr BP towards the present, which Clapperton et al. (1989) labelled the "Little Ice Age". However, the uncertainties in the age model for GC673 mean we cannot be certain if the apparent cooling occurred coeval with or prior to the Little Ice Age, but future studies may help clarify this. Van der Bilt et al. (2017) did report evidence of a two-stage Little Ice Age and glacial advancement around 0.3 and 0.12 cal. kyr BP on South Georgia, but our age model is not accurate enough to confirm this.

5 Conclusions

We carry out a multiproxy analysis of two cores off the east coast of South Georgia on the inner shelf (GC673) and mid-shelf (GC665) to reconstruct Holocene changes in marine primary productivity and relate them to the island's glacial history. The latest Pleistocene and earliest Holocene (ca. 15.2 to 10.8 cal. kyr BP) was a period of relatively high productivity associated with increased nutrient delivery likely from meltwater and glacial flour during deglaciation, as inferred from high BSi AR and C_{org} AR and dominance of the benthic foraminifera *F. fusiformis*. After reducing productivity, from ca. 8 to 3 cal. kyr BP, lower sedimentation rates, reduced nutrient delivery, and lower primary productivity represent a period of diminished overall glacial influence on the mid-shelf. However, the more nearshore GC673 documents at least three short-lived episodes of enhanced organic primary productivity indicated by dominant *F. fusiformis*, which we interpret to represent glacial readvances, allowing greater seasonal meltwater and associated iron delivery to GC673. During the late Holocene, there is evidence for an increase in productivity in GC673 and, to a lesser extent, in distal GC666, associated with cooling temperatures, a further readvance of glaciers, and associated with northward migration and strengthening of the SWWs which may have had a causal influence via precipitation.

In our study, the most useful benthic foraminifera as a productivity proxy is *F. fusiformis*, with higher relative abundances linked to higher productivity, as documented in our other productivity proxies BSi AR and C_{org} AR. High dominance ($> 60\,\%$) of *M. earlandi* and other agglutinated foraminifera appear to be a useful dissolution proxy in this setting. Carbonate dissolution horizons and diagenetic alteration are observed in both cores, especially from the Pleistocene through to the end of the mid-Holocene in GC666. The Pleistocene and early-Holocene dissolution appears to be related to high organic flux to the sea floor, while mid-Holocene dissolution may have been caused by low sedimentation rates.

Data availability. Raw radiocarbon dates with calibrations are available in Table 2 and dataset used and analysed are included in the Supplement.

Supplement. The supplement related to this article is available online at: https://doi.org/10.5194/jm-43-165-2024-supplement.

Author contributions. The research was carried out as part of PhD work by JTRW and RD. The study was conceptualised by SK, CSA, VLP, GEAS, and MJL. Benthic foraminiferal assemblage data were generated by JTRW and RD. Radiocarbon samples and age modelling was done by JTRW and RD. Biogenic silica was analysed by RD and GEAS. Stable isotope data was analysed by MJL. All authors contributed to data analysis and writing of the paper.

Competing interests. At least one of the (co-)authors is a member of the editorial board of *Journal of Micropalaeontology*. The peer-review process was guided by an independent editor, and the authors also have no other competing interests to declare.

Disclaimer. Publisher's note: Copernicus Publications remains neutral with regard to jurisdictional claims made in the text, published maps, institutional affiliations, or any other geographical representation in this paper. While Copernicus Publications makes every effort to include appropriate place names, the final responsibility lies with the authors.

Special issue statement. This article is part of the special issue "Advances in Antarctic chronology, paleoenvironment, and paleoclimate using microfossils: Results from recent coring campaigns". It is not associated with a conference.

Acknowledgements. Isotope measurements were performed by Hilary Sloane and Jack Lacey (University of Nottingham). Laboratory support at the University of Nottingham was provided by Teresa Needham and Ian Conway. We thank the captain, crew, and science party on board RRS *James Clark Ross* during cruise JR-257 for the acquisition of the material that forms the basis of this study. The R code was prepared by Fermin Alvarez Agoues (Trinity College Dublin), and Zoe Roseby (University of Exeter) kindly

helped with the age–depth modelling. Radiocarbon dates were conducted at the Ion Beam Laboratory (ETH Zürich, Switzerland), the Poznan Radiocarbon Laboratory (Adam Mickiewicz University, Poland), and the NERC Radiocarbon Facility (East Kilbride, UK). We would also like to thank the three reviewers, Michael A. Kaminski (King Fahd University of Petroleum and Minerals, Dhahran), Caterina Morigi (Università di Pisa), and the anonymous reviewer, who all provided incredibly helpful comments for the paper. Finally, we would like to thank Francesca Sangiorgi (Utrecht University) for her help in her capacity as the editor of this work.

Financial support. This research has been supported by the Leverhulme Trust 5 (grant no. RF-2020-447/4; Sev Kender), the Natural Environment Research Council (NERC Isotope Geoscience Facility Grant (grant no. IP/1495/1114; Melanie L. Leng), and the NERC Radiocarbon Facility Steering Committee (grant no. 1944.1015; Rowan Dejardin).

Review statement. This paper was edited by Francesca Sangiorgi and reviewed by Michael Kaminski and one anonymous referee.

References

Ahn, S., Khider, D., Lisiecki, L. E., and Lawrence, C. E.: A probabilistic Pliocene–Pleistocene stack of benthic $\delta^{18}O$ using a profile hidden Markov model, Dynam. Stat. Clim. Syst., 2, dzx002, https://doi.org/10.1093/climsys/dzx002, 2017.

Allen, C. S., Peck, V. L., Graham, A. G. C., Blagbrough, H., Robinson, M. W., and McClymont, E.: Collecting records of past oceanographic conditions and calibrating new proxies in the Polar Front Zone of the SW Atlantic (Falkland Plateau, Shag Rocks and South Georgia), Cruise Report (JR-257), British Antarctic Survey, https://www.bodc.ac.uk/resources/inventories/cruise_inventory/reports/jr257_254e.pdf (last access: 14 June 2024), 2012.

Alve, E.: Foraminifera, climatic change, and pollution: a study of late Holocene sediments in Drammensfiord, southeast Norway, The Holocene, 1, 243–262, https://doi.org/10.1177/095968369100100306, 1991.

Alve, E.: Benthic foraminiferal distribution and recolonization of formerly anoxic environments in Drammensfjord, southern Norway, Mar. Micropaleontol., 25, 169–186, https://doi.org/10.1016/0377-8398(95)00007-N, 1995.

Anderson, J. B.: Ecology and distribution of foraminifera in the Weddell Sea of Antarctica, Micropalaeontology, 21, 69–96, https://doi.org/10.2307/1485156, 1975.

Anderson, R. F., Ali, S., Bradtmiller, L. I., Nielsen, S. H. H., Fleisher, M. Q., Anderson, B. E., and Burckle, L. H.: Wind-Driven Upwelling in the Southern Ocean and the Deglacial Rise in Atmospheric CO_2, Science, 323, 1443–1448, https://doi.org/10.1126/science.1167441, 2009.

Ardelan, M. V., Holm-Hansen, O., Hewes, C. D., Reiss, C. S., Silva, N. S., Dulaiova, H., Steinnes, E., and Sakshaug, E.: Natural iron enrichment around the Antarctic Peninsula in the Southern Ocean, Biogeosciences, 7, 11–25, https://doi.org/10.5194/bg-7-11-2010, 2010.

Atkinson, A., Whitehouse, M. J., Priddle, J., Cripps, G. C., Ward, P., and Brandon, M. A.: South Georgia, Antarctica: a productive, cold water, pelagic ecosystem, Mar. Ecol. Prog. Ser., 216, 279–308, http://https://doi.org/10.3354/meps216279, 2001.

Bakke, J., Paasche, Ø., Schaefer, J. M., and Timmermann, A.: Long-term demise of sub-Antarctic glaciers modulated by the Southern Hemisphere Westerlies, Sci. Rep., 11, 8361, https://doi.org/10.1038/s41598-021-87317-5, 2021.

Barlow, N. L. M., Bentley, M. J., Spada, G., Evans, D. J. A., Hansom, J. D., Brader, M. D., White, D. A., Zander, A., and Berg, S.: Testing models of ice cap extent, South Georgia, sub-Antarctic, Quaternary Sci. Rev., 154, 157–168, https://doi.org/10.1016/j.quascirev.2016.11.007, 2016.

Barnes, D. K. A., Sands, C. J., Hogg, O. T., Robinson, B. J. O., Downey, R. V., and Smith, J. A.: Biodiversity signature of the Last Glacial Maximum at South Georgia, Southern Ocean, J. Biogeogr., 43, 2391–2399, http://https://doi.org/10.1111/jbi.12855, 2016.

Björck. S., Rundgren, M., Ljung, K., Unkel, I., and Wallin, Å.: Multi-proxy analyses of a peat bog on Isla de los Estados, easternmost Tierra del Fuego: a unique record of the variable Southern Hemisphere Westerlies since the last deglaciation, Quaternary Sci. Rev., 42, 1–14, https://doi.org/10.1016/j.quascirev.2012.03.015, 2014.

Borrione, I., Aumont, O., Nielsdóttir, M. C., and Schlitzer, R.: Sedimentary and atmospheric sources of iron around South Georgia, Southern Ocean: a modelling perspective, Biogeosciences, 11, 1981–2001, https://doi.org/10.5194/bg-11-1981-2014, 2014.

Bentley, M. J., Evans, D. J. A., Fogwill, C. J., Hansom, J. D., Sugden, D. E., and Kubik, P. W.: Glacial geomorphology and chronology of deglaciation, South Georgia, sub-Antarctic, Quaternary Sci. Rev., 26, 644–677, https://doi.org/10.1016/j.quascirev.2006.11.019, 2007.

Berg, S., White, D. A., Jivcov, S., Melles, M., Leng, M. J., Rethemeyer, J., Allen, C., Perren, B., Bennike, O., and Viehberg, F.: Holocene glacier fluctuations and environmental changes in subantarctic South Georgia inferred from a sediment record from a coastal inlet, Quaternary Res., 91, 132–148, https://doi.org/10.1017/qua.2018.85, 2019.

Bracegirdle, T.: Southern Hemisphere tropospheric westerly jet: 1979-present, Polar Data Centre, Natural Environment Research Council, UK, https://doi.org/10.5285/3952a4fe-683a-42e7-a074-bdec41c8ab16, 2023.

Browne, I. M., Moy, C. M., Riesselman, C. R., Neil, H. L., Curtin, L. G., Gorman, A. R., and Wilson, G. S.: Late Holocene intensification of the westerly winds at the subantarctic Auckland Islands (51° S), New Zealand, Clim. Past 13, 1301–1322, https://doi.org/10.5194/cp-13-1301-2017, 2017.

Ciais, P., Petit, J. R., Jouzel, J., Lorius, C., Barkov, N. I., Lipenkov, V., and Nicolaïev, V.: Evidence for an early Holocene climatic optimum in the Antarctic deep ice-core record, Clim. Dynam., 6, 169–177, https://doi.org/10.1007/BF00193529, 1992.

Clapperton, C. M., Sugen, D. E., Birnie, J., and Wilson, M. J.: Late-Glacial and Holocene glacier fluctuations and environmental change on South Georgia, Southern Ocean, Quaternary Res., 31, 210–228, https://doi.org/10.1016/0033-5894(89)90006-9, 1989.

Clark, P. U., Dyke, A. S., Shakun, J. D., Carlson, A. E., Clark, J., Wohlfarth, B., Mitrovica, J. X., Hostetler, S. W., and Mc-

Cabe, A. M.: The Last Glacial Maximum, Science, 325, 710–714, https://doi.org/10.1126/science.1172873, 2009.

Clark, P. U., McCabe, A. M., Mix, A. C., and Weaver, A. J.: Rapid rise of sea level 19,000 years ago and its global implications, Science, 304, 1141–1144, https://doi.org/10.1126/science.1094449, 2004.

Clark, P. U., Shakun, J. D., Baker, P. A., Bartlein, P. J., Brewer, S., Brook, E., Carlson, A. E., Cheng, H., Kaufman, D. S., Liu, Z., Marchitto, T. M., Mix, A. C., Morrill, C., Otto-Bliesner, B. L., Pahnke, K., Russell, J. M., Whitlock, C., Adkins, J. F., Blois, J. L., Clark, J., Colman, S. M., Curry, W. B., Flower, B. P., He, F., Johnson, T. C., Lynch-Stieglitz, J., Markgraf, V., McManus, J., Mitrovica, J. X., Moreno, P. I., and Williams, J. W.: Global climate evolution during the last deglaciation, Proceedings of the National Academy of Sciences, 109, E1134–E1142, https://doi.org/10.1073/pnas.1116619109, 2012.

Combes, V., Matano, R. P., Meredith, M. P., and Young, E. F.: Variability of the shelf circulation around South Georgia, Southern Ocean, J. Geophys. Res.-Ocean., 128, e2022JC019257, https://doi.org/10.1029/2022JC019257, 2023.

Conley, D. J. and Schelske, C. L.: Biogenic Silica, in: Tracking environmental change using lake sediments, Vol. 3, terrestrial, algal, and siliceous indicators, edited by: Smol, J. P., Birks, H. J. B., and Last, W. M., Kluwer Academic, Dordrecht, Netherlands, 281–293, https://doi.org/10.1007/0-306-47668-1_14, 2001.

Dejardin, R.: Reconstructing oceanographic conditions through the deglacial and Holocene (ca. 15 KA) at the sub-Antarctic island of South Georgia, Ph.D. thesis, University of Nottingham, United Kingdom, 257 pp., 2017.

Dejardin, R., Kender, S., Allen, C. S., Leng, M. J., Swann, G. E. A., and Peck, V. L.: "Live" (stained) benthic foraminiferal living depths, stable isotopes, and taxonomy offshore South Georgia, Southern Ocean: implications for calcification depths, J. Micropalaeontol., 37, 25–71, https://doi.org/10.5194/jm-37-25-2018, 2018.

Demaster, D. J.: The supply and accumulation of silica in the marine environment, Geochim. Cosmochim. Ac., 45, 1715–1732, https://doi.org/10.1016/0016-7037(81)90006-5, 1981.

Detlef, H., Sosdian, S. M., Kender, S., Lear, C. H., and Hall, I. R.: Multi-elemental composition of authigenic carbonates in benthic foraminifera from the eastern Bering Sea continental margin (International Ocean Discovery Program Site U1343), Geochim. Cosmochim. Ac., 268, 1–21, https://doi.org/10.1016/j.gca.2019.09.025, 2020.

Divine, D. V., Koç, N., Isaksson, E., Nielsen, S., Crosta, X., and Godtliebsen, F.: Holocene Antarctic climate variability from ice and marine sediment cores: Insights on ocean–atmosphere interaction, Quaternary Sci. Rev., 29, 303–312, https://doi.org/10.1016/j.quascirev.2009.11.012, 2010.

Favier, L., Pattyn, F., Berger, S., and Drews, R.: Dynamic influence of pinning points on marine ice-sheet stability: a numerical study in Dronning Maud Land, East Antarctica, The Cryosphere, 10, 2623–2635, https://doi.org/10.5194/tc-10-2623-2016, 2016.

Fisher, R. A., Corbet, A. S., and Williams, C. B.: The relation between the number of species and the number of individuals in a random sample of an animal population, J. Anim. Ecol., 12, 42–58, https://doi.org/10.2307/1411, 1943.

Fletcher, M.-S., Pedro, J., Hall, T., Mariani, M., Alexander, J. A., Beck, K., Blaauw, M., Hodgson, D. A., Heijnis, H., Gadd, P. S., and Lise-Pronovost, A.: Northward shift of the southern westerlies during the Antarctic Cold Reversal, Quaternary Sci. Rev., 271, 107189, https://doi.org/10.1016/j.quascirev.2021.107189, 2021.

Foster, L. C., Pearson, E. J., Juggins, S., Hodgson, D. A., Saunders, K. M., Verleyen, E., and Roberts, S. J.: Development of a regional glycerol dialkyl glycerol tetraether (GDGT)–temperature calibration for Antarctic and sub-Antarctic lakes, Earth Planet. Sc. Lett., 433, 370–379, https://doi.org/10.1016/j.epsl.2015.11.018, 2016.

Graham, A. G. C., Fretwell, P. T., Larter, R. D., Hodgson, D. A., Wilson, C. K., Tate, A. J., and Morris, P.: A new bathymetric compilation highlighting extensive paleo–ice sheet drainage on the continental shelf, South Georgia, sub-Antarctica, Geochem. Geophy. Geosy., 9, Q07011, https://doi.org/10.1029/2008GC001993, 2008.

Graham, A. G. C., Kuhn, G., Meisel, O., Hillenbrand, C.-D., Hodgson, D. A., Ehrmann, W., Wacker, L., Wintersteller, P., dos Santos Ferreira, C., Römer, M., White, D., and Bohrmann, G.: Major advance of South Georgia glaciers during the Antarctic Cold Reversal following extensive sub-Antarctic glaciation, Nat. Commun., 8, 14798, https://doi.org/10.1038/ncomms14798, 2017.

Gordon, J. E., Haynes, V., and Hubbard, A.: Recent glacier changes and climate trends on South Georgia, Glob. Planet. Change, 60, 72–84, https://doi.org/10.1016/j.gloplacha.2006.07.037, 2008.

Hall, B. L.: Holocene glacial history of Antarctica and the sub-Antarctic islands, Quaternary Sci. Rev., 28, 2213–2230, https://doi.org/10.1016/j.quascirev.2009.06.011, 2009.

Hammer, Ø.: PAleontological STatistics version 4.10 reference manual, https://www.nhm.uio.no/english/research/infrastructure/past/downloads/past4manual.pdf (last access: 13 July 2023), 2022.

Haslett, J. and Parnell, A. C.: A simple monotone process with application to radiocarbon-dated depth chronologies, J. Roy. Stat. Soc. Ser. C, 57, 399–418, https://doi.org/10.1111/j.1467-9876.2008.00623.x, 2008.

Heaton, T. J., Köhl, P., Butzin, M., Bard, E., Reimer, R. W., Austin, W. E. N., Bronk Ramsey, C., Grootes, P. M., Hughen, K. A., Kromer, B., Reimer, P. J., Adkins, J., Burke, A., Cook, M. S., Olsen, J., and Skinner, L. C.: Marine20-The marine radiocarbon age calibration curve (0–55,000 cal BP), Radiocarbon, 62, 779–820, https://doi.org/10.1017/RDC.2020.68, 2020.

Hein, J. R., Oneil, J. R., and Jones, M. G.: Origin of authigenic carbonates in sediment from the deep Bering Sea, Sedimentology, 26, 681–705, https://doi.org/10.1111/j.1365-3091.1979.tb00937.x, 1979.

Hill, M. O. and Gauch Jr., H. G.: Detrended Correspondence analysis: an improved ordination technique, Vegetatio, 42, 47–58, https://doi.org/10.1007/BF00048870, 1980.

Hodgson, D. A., Graham, A. G. C., Roberts, S. J., Bentley, M. J., Ó Cofaigh, C., Verleyen, E., Vyverman, W., Jomelli, V., Favier, V., runstein, D., Verfaillie, D., Colhoun, E. A., Saunders, K. M., Selkirk, P. M., Mackintosh, A., Hedding, D. W., Nel, W., Hall, K., McGlone, M. S., van der Putten, N., Dickens, W. A., and Smith, J. A.: Terrestrial and submarine evidence for the extent and timing of the Last Glacial Maximum and the onset of deglaciation on the maritime-Antarctic and sub-Antarctic islands, Quaternary Sci. Rev., 100, 137–158, https://doi.org/10.1016/j.quascirev.2013.12.001, 2014a.

Hodgson, D. A., Graham, A. G., Griffiths, H. J., Roberts, S. J., Cofaigh, C.Ó., Bentley, M. J., and Evans, D. J.: Glacial history of sub-Antarctic South Georgia based on the sub-marine geomorphology of its fjords, Quaternary Sci. Rev., 89, 129–147, https://doi.org/10.1016/j.quascirev.2013.12.005, 2014b.

Ishman, S. E. and Sperling, M. R.: Benthic foraminiferal record of Holocene deep-water evolution in the Palmer Deep, western Antarctic Peninsula, Geology, 30, 435–438, 2002.

Kilfeather, A. A., O Cofaigh, C., Lloyd, J. M., Dowdeswell, J. A., Xu, S., and Moreton, S. G.: Ice-stream retreat and ice-shelf history in Marguerite Trough, Antarctic Peninsula: Sedimentological and foraminiferal signatures, Geol. Soc. Am. Bull., 123, 997–1015, https://doi.org/10.1130/B30282.1, 2011.

Kristan, A. K., Maiti, K., McMahon, K. W., Dance, M. A., and Polito, M. J.: Biological and geochemical proxies in sediment cores reveal shifts in marine predator population dynamics relative to historic anthropogenic exploitation and recent climate change at South Georgia Island sub-Antarctic, Polar Biol., 45, 1379–1389, https://doi.org/10.1007/s00300-022-03067-8, 2022.

Lamy, F., Kilian, R., Arz, H. W., Francois, J.-P., Kaiser, J., Prange, M., and Steinke, T.: Holocene changes in the position and intensity of the southern westerly wind belt, Nat. Geosci., 3, 695–699, https://doi.org/10.1038/ngeo959, 2010.

Lešić, N.-M., Streuff, K. T., Bohrmann, G., and Kuhn, G.: Glacimarine sediments from outer Drygalski Trough, sub-Antarctic South Georgia – evidence for extensive glaciation during the Last Glacial Maximum, Quaternary Sci. Rev., 292, 107657, https://doi.org/10.1016/j.quascirev.2022.107657, 2022.

Li, B. H., Yoon, H. I., and Park, B. K.: Foraminiferal assemblages and $CaCO_3$ dissolution since the last deglaciation in the Maxwell Bay, King George Island, Antarctica, Mar. Geol., 169, 239–257, https://doi.org/10.1016/S0025-3227(00)00059-1, 2000.

Lisiecki, L. E. and Raymo, M. E.: A Pliocene-Pleistocene stack of 57 globally distributed benthic $\delta^{18}O$ records, Paleoceanogr. Paleocl., 20, PA1003, https://doi.org/10.1029/2004PA001071, 2005.

Mackensen, A., Schmeidl, G., Harloff, J., and Giese, M.: Deep-sea foraminifera in the South Atlantic Ocean: ecology and assemblage generation, Micropaleontology, 41, 342–358, https://doi.org/10.2307/1485808, 1995.

Majewski, W.: Benthic foraminiferal communities: distribution and ecology in Admiralty Bay, King George Island, West Antarctica, Pol. Polar Res., 26, 159–214, 2005.

Majewski, W.: Benthic foraminifera from West Antarctic fjord environments: An overview, Pol. Polar Res., 31, 61–82, https://journals.pan.pl/publication/124133, 2010.

Majewski, W. and Anderson, J. B.: Holocene foraminiferal assemblages from Firth of Tay, Antarctic Peninsula: Paleoclimate implications, Mar. Micropaleontol., 73, 135–147, https://doi.org/10.1016/j.marmicro.2009.08.003, 2009.

Majewski, W., Wellner, J. S., Szczuciński, W., and Anderson, J. B.: Holocene oceanographic and glacial changes recorded in Maxwell Bay, West Antarctica, Mar. Geol., 326–328, 67–79, https://doi.org/10.1016/j.margeo.2012.08.009, 2012.

Majewski, W., Wellner, J. S., and Anderson, J. B.: Environmental connotations of benthic foraminiferal assemblages from coastal West Antarctica, Mar. Micropaleontol., 124, 1–15, https://doi.org/10.1016/j.marmicro.2016.01.002, 2016.

Majewski, W., Szczuciński, W., and Gooday, A. J.: Unique benthic foraminiferal communities (stained) in diverse environments of sub-Antarctic fjords, South Georgia, Biogeoscience, 20, 523–544, https://doi.org/10.5194/bg-20-523-2023, 2023.

Masson, V., Vimeux, F., Jouzel, J., Morgan, V., Delmotte, M., Ciais, P., Hammer, C., Johnsen, S., Lipenkov, V. Y., Mosely-Thompson, E., Petit, J.-R., Steig, E. J., Stievenard, M., and Viakmae, R.: Holocene climate variability in Antarctica based on 11 ice-core isotopic records, Quaternary Res., 54, 348–358, https://doi.org/10.1006/qres.2000.2172, 2000.

Mayr, C., Wille, M., Haberzettl, T., Fey, M., Janssen, S., Lücke, A., Ohlendorf, C., Oliva, G., Schäbitz, F., Schleser, G. H., and Zolitschka, B.: Holocene variability of the Southern Hemisphere westerlies in Argentinean Patagonia (52° S), Quaternary Sci. Rev., 26, 579–584, https://doi.org/10.1016/j.quascirev.2006.11.013, 2007.

Meisel, O. H., Graham, A. G. C., and Kuhn, G.: A new record of post-glacial sedimentation in a glacial trough, offshore sub- =Antarctic South Georgia, EGU General Assembly 2014, Vienna, Austria, 27 April–2 May 2014, EGU2014-10852, https://meetingorganizer.copernicus.org/EGU2014/EGU2014-10852.pdf (last access: 14 June 2024), 2014.

Menounos, B., Clague, J. J., Osborn, G., Davis, P. T., Ponce, F., Goehring, B., Maurer, M., Rabassa, J., Coronato, A., and Marr, R.: Latest Pleistocene and Holocene glacier fluctuations in southernmost Tierra del Fuego, Argentina, Quaternary Sci. Rev., 77, 70–79, https://doi.org/10.1016/j.quascirev.2013.07.008, 2013.

Meredith, M. P., Watkins, J. L., Murphy, E. J., Ward, P., Bone, D. G., Thorpe, S. E., Grant, S. A., and Ladkin, R. S.: Southern ACC front to the northeast of South Georgia: Pathways, characteristics, and fluxes, J. Geophys. Res.-Ocean., 108, 3162, https://doi.org/10.1029/2001JC001227, 2003.

Milam, R. W. and Anderson, J. B.: Distribution and ecology of Recent benthonic foraminifera of the Adelie – George V continental shelf and slope, Antarctic, Mar. Micropaleontol., 6, 297–325, https://doi.org/10.1016/0031-0182(79)90107-X, 1981.

Mulvaney, R., Abram, N. J., Hindmarsh, R. C. A., Arrowsmith, C., Fleet, L., Triest, J., Sime, L. C., Alemany, O., and Foord, S.: Recent Antarctic Peninsula warming relative to Holocene climate and ice-shelf history, Nature, 489, 141–144, https://doi.org/10.1038/nature11391, 2012.

Nielsdóttir, M. C., Bibby, T. S., Moore, C. M., Hinz, D. J., Sanders, R., Whitehouse, M., Korb, R., and Achterberg, E. P.: Seasonal and spatial dynamics of iron availability in the Scotia Sea, Mar. Chem., 130/131, 62–72, https://doi.org/10.1016/j.marchem.2011.12.004, 2012.

Oksman, M., Kvorning, A. B., Larsen, S. H., Kjeldsen, K. K., Mankoff, K. D., Colgan, W., Andersen, T. J., Nørgaard-Pedersen, N., Seidenkrantz, M.-S., Mikkelsen, N., and Ribeiro.: Impact of freshwater runoff from the southwest Greenland Ice Sheet on fjord productivity since the late 19th century, The Cryosphere, 16, 2471–2491, https://doi.org/10.5194/tc-16-2471-2022, 2022.

Oppedal, L. T., Bakke, J., Paasche, Ø., Werner, J. P., and van der Bilt, E. G. M.: Cirque glacier on South Georgia shows centennial variability over the last 7000 years, Front. Earth Sci., 6, 1–18, https://doi.org/10.3389/feart.2018.00002, 2018.

Oksanen, J. and Minchin, P. R.: Instability of ordination results under changes in input data order: explanations and remedies, J. Veg. Sci., 8, 447–454, https://doi.org/10.2307/3237336, 1997.

Peck, V. L., Allen, C. S., Kender, S., McClymont, E. L., and Hodgson, D.: Oceanographic variability on the West Antarc-

tic Peninsula during the Holocene and the influence of upper circumpolar deep water, Quaternary Sci. Rev., 119, 54–65, https://doi.org/10.1016/j.quascirev.2015.04.002, 2015.

Pedro, J. B., Bostock, H. C., Bitz, C. M., He, F., Vandergoes, M. J., Steig, E. J., Chase, B. M., Krause, C. E., Rasmussen, S. O., Markle, B. R., and Cortese, G.: The spatial extent and dynamics of the Antarctic Cold Reversal, Nat. Geosci., 9, 51–55, https://doi.org/10.1038/ngeo2580, 2016.

Perren, B. B., Hodgson, D. A., Roberts, S. J., Sime, L., van Nieuwenhuyze, W., Verleyen, E., and Vyverman, W.: Southward migration of the Southern Hemisphere westerly winds corresponds with warming climate over centennial timescales, Commun. Earth Environ., 1, 58, https://doi.org/10.1038/s43247-020-00059-6, 2020.

Pike, J. and Kemp, A. E. S.: Diatom mats in Gulf of California sediments: Implications for the paleoenvironmental interpretation of laminated sediments and silica burial, Geology, 27, 311–314, https://doi.org/10.1130/0091-7613(1999)027<0311:DMIGOC>2.3.CO;2, 1999.

Pohlman, J. W., Riedel, M., Bauer, J. E., Canuel, E. A., Paull, C. K., Lapham, L., Grabowski, K. S., Coffin, R. B., and Spence, G. D.: Anaerobic methane oxidation in low-organic content methane seep sediments, Geochim. Cosmochim. Ac., 108, 184–201, https://doi.org/10.1016/j.gca.2013.01.022, 2013.

Putnam, A. E., Denton, G. H., Schaefer, J. M., Barrell, D. J. A., Andersen, B. G., Finkel, R. C., Schwartz, R., Doughty, A. M., Kaplan, M. R., and Schluchter, C.: Glacier advance in southern middle-latitudes during the Antarctic Cold Reversal, Nat. Geosci., 3, 700–704, https://doi.org/10.1038/ngeo962, 2010.

Roberts, S. J., Hodgson, D. A., Shelley, S., Royles, J., Griffiths, H. J., Deen, T. J., and Thorne, M. A. S.: Establishing lichenometric ages for nineteenth- and twentieth-century glacier fluctuations on South Georgia (South Atlantic), Geogr. Ann. S. A Phys. Geogr., 92, 125–139, https://doi.org/10.1111/j.1468-0459.2010.00382.x, 2010.

Rodrigues, A. R., Malus, J. C. C., de Santis Braga, E., and Eichler, B. B.: Recent benthic foraminiferal distribution and related environmental factors in Ezcurra Inlet, King George Island, Antarctica, Antarct. Sci., 22, 343–360, https://doi.org/10.1017/S0954102010000179, 2010.

Römer, M., Torres, M., Kasten, S., Kuhn, G., Graham, A. G. C., Mau, S., Little, C. T. S., Linse, K., Pape, T., Geprägs, P., Fischer, D., Wintersteller, P., Marcon, Y., Rethemeyer, J., and Bohrmann, G.: First evidence of widespread active methane seepage in the Southern Ocean, off the sub-Antarctic island of South Georgia, Earth Planet. Sc. Lett., 403, 166–177, https://doi.org/10.1016/j.epsl.2014.06.036, 2014.

Rosqvist, G. C., Rietti-Shati, M., and Shemesh, A.: Late glacial to middle Holocene climatic record of lacustrine biogenic silica oxygen isotopes from a Southern Ocean island, Geology, 27, 967–970, https://doi.org/10.1130/0091-7613(1999)027<0967:LGTMHC>2.3.CO;2, 1999.

Schlosser, C., Schmidt, K., Aquilina, A., Homoky, W. B., Castrillejo, M., Mills, R. A., Patey, M. D., Fielding, S., Atkinson, A., and Achterberg, E. P.: Mechanisms of dissolved and labile particulate iron supply to shelf waters and phytoplankton blooms off South Georgia, Southern Ocean, Biogeosciences, 15, 4973–4993, https://doi.org/10.5194/bg-15-4973-2018, 2018.

Schneider, A., Crémière, A., Panieri, G., Lepland, A., and Knies, J.: Diagenetic alteration of benthic foraminifera from a methane seep site on the Vestnesa Ridge (NW Svalbard margin), Deep-Sea Res. Pt. I, 123, 22–34, https://doi.org/10.1016/j.dsr.2017.03.001, 2017.

Schmiedl, G. and Leuschner, D. C.: Oxygenation changes in the deep western Arabian Sea during the last 190,000 years: Productivity versus deepwater circulation, Paleoceanography, 20, PA2008, https://doi.org/10.1029/2004PA001044, 2005.

Skinner, L. C., Muschitiello, F., and Scrivner, A. E.: Marine reservoir age variability over the last deglaciation: Implications for marine carbon cycling and prospects for regional radiocarbon calibrations, Paleoceanogr. Paleocl., 34, 1807–1815, https://doi.org/10.1029/2019PA003667, 2019.

Spoth, M., Hall, B., Lowell, T., Diefendorf, A. F., Corcoran, M. C., and Brickle, P.: Tracking the southern hemisphere westerlies during and since the last glacial maximum with multiproxy lake records from the Falkland Islands (52° S), Quaternary Sci. Rev., 311, 108135, https://doi.org/10.1016/j.quascirev.2023.108135, 2023.

Strelin, J. A., Kaplan, M. R., Vandergoes, M. J., Denton, H. G., and Schaefer, J. M.: Holocene glacier history of the Lago Argentino basin, Southern Patagonian Icefield, Quaternary Sci. Rev., 101, 124–145, https://doi.org/10.1016/j.quascirev.2014.06.026, 2014.

Strother, S. L., Salzmann, U., Roberts, S. J., Hodgson, D. A., Woodward, J., Nieuwenhuyze, W. V., Verleyen, E., Vyverman, W., and Moreton, S. G.: Changes in Holocene climate and the intensity of Southern Hemisphere Westerly Winds based on a high-resolution palynological record from sub-Antarctic South Georgia, Holocene, 25, 263–279, https://doi.org/10.1177/0959683614557576, 2015.

Toggweiler, J. R., Russell, J. L., and Carson, S. R.: Midlatitude westerlies, atmospheric CO_2, and climate change during the ice ages, Paleoceanography, 21, PA2005, https://doi.org/10.1029/2005PA001154, 2006.

van der Bilt, W. G. M., D'Andrea, W. J., Oppedal, L. T., Bakke, J., Bjune, A. E., and Zwier, M.: Stable Southern Hemisphere westerly winds throughout the Holocene until intensification in the last two millennia, Commun. Earth Environ., 3, 186, https://doi.org/10.1038/s43247-022-00512-8, 2022.

van der Putten, N. and Verbruggen, C.: The onset of deglaciation of Cumberland Bay and Stromness Bay, South Georgia, Antarct. Sci., 17, 29–32, https://doi.org/10.1017/S0954102005002397, 2005.

van der Putten, N., Stieperaere, H., Verbruggen, C., and Ochyra, R.: Holocene palaeoecology and climate history of South Georgia (sub-Antarctica) based on a macrofossil record of bryophytes and seeds, Holocene, 14, 382–392, https://doi.org/10.1191/0959683604hl714rp, 2004.

White, D. A., Bennike, O., Melles, M., Berg, S., and Binnie, S. A.: Was South Georgia covered by an ice cap during the Last Glacial Maximum?, Geol. Soc. Lond. Sp. Publ., 461, 49–59, https://doi.org/10.1144/SP461.4, 2018.

Wycech, J., Kelly, D. C., and Marcott, S.: Effects of seafloor diagenesis on planktic foraminiferal radiocarbon ages, Geology, 44, 551–554, https://doi.org/10.1130/G37864.1, 2016.

Xia, Z., Oppedal, L. T., van der Putten, N., Bakker, J., and Yu, Z.: Ecological response of a glacier-fed peatland to late Holocene climate and glacier changes on subantarc-

tic South Georgia, Quaternary Sci. Rev., 250, 1066792, https://doi.org/10.1016/j.quascirev.2020.106679, 2020.

Xiao, W., Esper, O., and Gersonde, R.: Last Glacial-Holocene climate variability in the Atlantic sector of the Southern Ocean, Quaternary Sci. Rev., 135, 115–137, https://doi.org/10.1016/j.quascirev.2016.01.023, 2016.

Zwier, M., van der Bilt, W. G. M., de Stigter, H., and Bjune, A. E.: Pollen evidence of variations in Holocene climate and Southern Hemisphere Westerly Wind strength on sub-Antarctic South Georgia, Holocene, 32, 147–158, https://doi.org/10.1177/09596836211060495, 2021.